Glucocorticoid receptor antagonization propels endogenous cardiomyocyte proliferation and cardiac regeneration

Glucocorticoid Receptor antagonization propels endogenous cardiomyocyte proliferation and cardiac regeneration

Nicola Pianca[1,#], Francesca Sacchi[2,3,4,#], Kfir-Baruch Umansky[5], Maila Chirivì[6,7], Luisa Iommarini[8], Silvia Da Pra[2,3,4], Valentina Papa[9], Chiara Bongiovanni[2,3,4], Carmen Miano[4,3], Francesca Pontis[1], Luca Braga[10], Riccardo Tassinari[11], Elvira Pantano[1], Rahul Shastry Patnala[1], Martina Mazzeschi[2], Giovanna Cenacchi[9], Anna Maria Porcelli[8], Mattia Lauriola[2], Carlo Ventura[2,4], Mauro Giacca[10], Roberto Rizzi[7,12], Eldad Tzahor[5] and Gabriele D'Uva[2,3,4]

[1] Scientific and Technological Pole, IRCCS MultiMedica, Milan, Italy;

[2] Department of Experimental, Diagnostic and Specialty Medicine, University of Bologna, Bologna, Italy

[3] Centre for Applied Biomedical Research (CRBA), University of Bologna, Bologna, Italy;

[4] National Laboratory of Molecular Biology and Stem Cell Engineering, National Institute of Biostructures and Biosystems (INBB), Bologna, Italy

[5] Department of Molecular Cell Biology, Weizmann Institute of Science, Rehovot, Israel

[6] Institute of Biochemistry and Cell Biology (IBBC), National Research Council of Italy (CNR), Monterotondo Scalo, Rome, Italy

[7] National Institute of Molecular Genetics (INGM) "Romeo ed Enrica Invernizzi", Milan, Italy

[8] Department of Pharmacy and Biotechnology, University of Bologna, Bologna, Italy

[9] Department of Biomedical and Neuromotors Sciences, Anatomic Pathology at S. Orsola Hospital, University of Bologna, Bologna, Italy

[10] British Heart Foundation Centre of Research Excellence, School of Cardiovascular Medicine & Sciences, King's College London, UK

[11] Eldor Lab c/o CNR, Via Gobetti 101, 40129 Bologna, Italy

[12] Institute of Biomedical Technologies (ITB), National Research Council of Italy (CNR), Segrate, Milan, Italy

[#] These authors contributed equally to this work.

Corresponding Author:

Gabriele D'Uva, PhD

Department of Experimental, Diagnostic and Specialty Medicine, University of Bologna, Bologna 40138, Italy. Email: gabrielematteo.duva2@unibo.it

ABSTRACT

In mammals, the physiological activation of the glucocorticoid receptor (GR) by glucocorticoids (GCs) promotes the maturation of cardiomyocytes during late gestation, but the impact on postnatal cardiac growth and regenerative plasticity is unclear.

Here, we demonstrate that GCs/GR axis restrains cardiomyocyte proliferation during postnatal development. Cardiomyocyte-specific GR ablation in mice (GR-cKO) delayed the postnatal cardiomyocyte cell cycle exit, hypertrophic growth and cytoarchitectural maturation. GR-cKO hearts showed increased expression of genes involved in glucose catabolism and reduced expression of genes promoting fatty acid oxidation and mitochondrial respiration. Accordingly, oxygen consumption in GR-cKO cardiomyocytes was less dependent on fatty acid oxidation, and glycolysis inhibition reverted GR-cKO effects on cardiomyocyte proliferation. GR ablation or transient pharmacological inhibition after myocardial infarction in juvenile and/or adult mice facilitated cardiomyocyte survival, cell cycle re-entry and division, leading to cardiac muscle regeneration along with reduced scar formation. Thus, GR restrains heart regeneration and may represent a therapeutic target.

INTRODUCTION

Heart disease is a leading cause of death. The loss of cardiac muscle cells (cardiomyocytes, CMs) after severe injuries, i.e. myocardial infarction, is a major cause of cardiac dysfunction and heart failure [1–5]. Intriguingly, lower vertebrates as well as mammals at foetal and neonatal stages robustly regenerate cardiac injuries by boosting endogenous cardiomyocyte proliferation [6–14]. Nevertheless, this ability in mammals is lost shortly after birth [6], when most cardiomyocytes permanently exit from the cell cycle [15,16]. Adult mammalian cardiomyocyte renewal is extremely low [17,18] and boosting cardiomyocyte proliferation is an emerging strategy to regenerate the damaged heart [1–5,19–23].

Glucocorticoids (GCs) are steroid hormones synthesised in the adrenal cortex and released into the circulatory system, exerting their actions through the Glucocorticoid Receptor (GR), and in some tissues or conditions through the Mineralocorticoid Receptor (MR) [24,25]. GR and MR reside and get activated directly in the intracellular space, then translocate to the nucleus and function as ligand-activated transcription factors. Physiological glucocorticoids (predominantly cortisol in mammals, including humans, and corticosterone in amphibians, reptiles, birds and rodents, including laboratory mice) influence many physiological processes, including development, immunity, inflammation, and stress response [24,25]. In mammals, circulating active glucocorticoids rise robustly in late gestation and are known to promote the maturation of the lungs and other organs to prepare the foetus for the postnatal life. During this prenatal developmental window, endogenous GCs were documented to induce the maturation of foetal cardiomyocytes via GR activation [24–26] as well as their proliferation through MR [27,28]. Other studies reported the adverse side-effects of synthetic GCs antenatal and/or neonatal therapies, resulting from an impairment in cardiomyocyte proliferation and endowment [29,30]. Very recently, the administration of synthetic GCs has been demonstrated to suppress cardiomyocyte regeneration at neonatal stage following injury in mice [31] and pigs [32].

Here, we sought to dissect the physiological role of endogenous GCs and their receptor GR on postnatal cardiomyocyte growth and maturation and regenerative potential during postnatal development and adult life. Our results support a model where GCs/GR axis restrains the proliferative and regenerative plasticity of cardiomyocytes. These effects were at least partially consequent to the modulation of the cellular energetic metabolism, from glycolysis to fatty acid oxidation. Hence, we propose that

the transient modulation of GR activity may represent a promising therapeutic approach for cardiomyocyte replacement upon cardiac injuries.

Results

Physiological glucocorticoids restrain neonatal cardiomyocyte proliferation via GR activation.

We first analysed the effect of corticosterone, the main endogenous glucocorticoid in rodents, on the proliferation of neonatal cardiomyocytes (postnatal day 1, P1). At this developmental stage, cardiomyocytes retain a certain degree of proliferation, reminiscent of the embryonic period. Cardiomyocyte proliferation was assessed by co-immunostaining for cardiomyocyte markers, namely cardiac troponin T (Tnnt2) or cardiac troponin I (Tnni3), together with proliferative markers, namely Ki67 for the active phases of the cell cycle and BrdU incorporation for cumulative analysis of cells that passed through S-phase. *In vitro* administration of corticosterone promoted a remarkable dose-dependent decrease in cardiomyocyte proliferation (**Figs. 1a-b**). Cardiomyocytes can undergo division of the nucleus (karyokinesis) without cytoplasm division (cytokinesis), which eventually leads to binucleation, a process linked to cardiomyocyte terminal differentiation. Thus, we also examined the effect of corticosterone on entering cytokinesis by the immunostaining of Aurora B kinase, which localizes at the central spindle during anaphase and at the cleavage furrow during cytokinesis. This analysis showed that the rate of cardiomyocyte cytokinesis was inhibited by the administration of a low dosage of corticosterone and completely suppressed by a high dosage (**Fig. 1c**). To directly visualize successful cell divisions, we employed time-lapse imaging of neonatal cardiomyocytes labelled with tetramethylrhodamine ethyl ester (TMRE) [33], following administration of corticosterone. Our analysis confirmed that the administration of corticosterone robustly inhibits cardiomyocyte cell division (**Fig. 1d**), without significantly impacting on cardiomyocyte binucleation (**Fig. 1e**). Representative videos of cardiomyocyte division and binucleation events are provided (**Supplementary Videos 1–2**).

Importantly, cotreatment with GR antagonist Mifepristone (RU486), but not with MR antagonist (eplerenone), abolished the suppressive effects of corticosterone on cardiomyocyte cell cycle re-entry (**Fig. 1f**) and DNA synthesis (**Fig. 1g**), suggesting the polarization through GR axis. Of note, administration of RU486 alone was able to boost cardiomyocyte cell cycle activity and proliferation (**Figs. 1f-g**). This effect likely

results from the antagonization of glucocorticoids contained in the horse serum in cardiomyocyte culture media (estimated to range from 4.5 to 8.8 nM, considering the concentrations reported in the literature [34,35] and the composition of our medium). Finally, a screening using EdU incorporation assay, performed with several FDA approved synthetic GR agonists, confirmed their shared ability to inhibit cardiomyocyte proliferation (**Fig. 1h**).

To evaluate the direct effect of corticosterone on cardiomyocyte proliferation, we performed a BrdU assay in cardiomyocyte-enriched compared to mixed cardiac cultures, observing similar repressive effects (**Extended Data Figs. 1a-b**). These data support a direct action of corticosterone on cardiomyocytes in inhibiting proliferation. Of note, corticosterone administration exerts an inhibitory effect also on stromal cells, although much lower compared to cardiomyocytes (**Extended Data Fig. 1c**). Indeed, low and high doses of corticosterone reduced stromal cell proliferation by ~20% and ~30%, whereas cardiomyocyte proliferation was reduced by ~47% and ~83%, respectively (see **Fig. 1b**).

These data demonstrate that physiological glucocorticoids facilitate cell cycle exit and reduce the proliferation of neonatal cardiomyocytes through specific activation of GR.

Glucocorticoids/GR axis concurs to postnatal cardiomyocyte cell cycle exit.

Most circulating glucocorticoids in the blood are bound to a transport protein termed corticosteroid-binding globulin (CBG, also known as transcortin) and to a lesser extent to albumin [36]. Only the unbound (free) fraction of cortisol is biologically active. Consequently, only a minor fraction (less than 10%) of the circulating corticosterone concentration is free to leave the circulation and to bind the glucocorticoid receptor in peripheral tissues [36]. Intriguingly, neonatal mice from birth up to 6 postnatal days were reported to exhibit no CBG activity [37]. Thus, in this developmental window, circulating corticosterone is free to diffuse into the peripheral tissues. The analysis of circulating corticosterone levels during postnatal development and in juvenile stages in mice evidenced a transient reduction of circulating corticosterone levels during the first week of postnatal life, likely consequent to the increased diffusion to the peripheral tissues (**Extended Data Fig. 1d**).

Next, we examined the dynamic regulation of GR expression levels within the cardiac tissue during the postnatal development and in juvenile stages. To this end, we first evaluated GR mRNA levels in P1, P3, P5, P7, P14, P28 and P56 heart lysates.

Intriguingly, our data revealed that mRNA expression of GR reaches a peak at P7, and it drops back to the P1 level in later postnatal stages (**Fig. 2a**). The same increase was also confirmed at protein level (**Fig. 2b**). Next, by immuno-magnetic cardiomyocytes purification, we confirmed that the change in GR expression was specific for cardiomyocytes rather than cardiac stromal cells (**Fig. 2c**). The quality of the fractionation procedure was validated by evaluating the expression levels of specific markers for cardiomyocytes (*Troponin T*), endothelial cells (*Pecam*) and fibroblasts (*Ddr2*) (**Extended Data Figs. 2a-c**). Nuclear localization of GR is associated with its activation and initiation of the transcriptional activity. To clarify the activation status of GR *in vivo* during early postnatal development, we analysed its nuclear staining in heart sections derived from postnatal day 1 (P1) and postnatal day 7 (P7) mice. GR appeared localized in the nucleus in most cardiomyocytes in both P1 and P7 mice (**Fig. 2d**), suggesting that GR is active at both stages.

To assess the impact of endogenous GCs/GR axis on cardiomyocyte cell cycle activity during the early postnatal development, we performed a pharmacological inhibition of GR by RU486 delivery in the first week after birth in mice. Our data showed that pups receiving RU486 had increased percentage of cycling cardiomyocytes (**Fig. 2e**), confirming the ability of the endogenous GCs/GR axis in promoting cell cycle exit during the early postnatal life.

Overall, these data suggest that a transient increase in GR abundance in cardiomyocytes coupled with high levels of free corticosterone, likely boosts GR axis to promote cardiomyocyte cell cycle exit during the early postnatal period.

Cardiomyocyte-specific GR deletion increases neonatal cardiomyocyte proliferation.

To evaluate the direct role of GR on cardiomyocyte proliferation, we generated a cardiomyocyte-specific GR conditional knock-out mouse model (GR-cKO mice) by crossing floxed GR mice (GR-loxP/loxP), which contain loxP sites flanking exon 3 of the GR gene, with mice expressing Cre recombinase under the control of the cardiac alpha myosin heavy chain promoter (αMyh6-Cre +/-) (**Fig. 3a**). GR-cKO mice were previously reported with normal morphology and heart function till adulthood (2 months of age) [38]; however, the potential impact on postnatal cardiomyocyte proliferation was unclear. Cardiac GR ablation was confirmed at the protein level by western blot analysis (**Fig. 3b**) and immunofluorescence analysis of cardiomyocytes

isolated from neonatal GR-cKO mice confirmed that the deletion occurred specifically in cardiomyocytes (**Extended Data Fig. 3a**). Importantly, GR-cKO cultured neonatal (P1) cardiomyocytes displayed higher proliferation rates compared to the control counterpart, in terms of cell cycle activity (**Fig. 3c**), DNA synthesis (**Fig. 3d**) and cytokinesis (**Fig. 3e**). Furthermore, time lapse analysis of cell division events in CMs isolated from P1 control and GR-cKO mice confirmed that GR ablation is sufficient to increase cardiomyocyte division (**Fig. 3f**), with a modest tendency towards a reduction in cardiomyocyte binucleation (**Fig. 3g**). Representative videos of cardiomyocyte division and binucleation events are provided (**Supplementary Videos 3-4**). These data clearly demonstrate that GR restrains cell cycle activity and proliferation of immature neonatal cardiomyocytes.

GR-cKO delays the postnatal transition from hyperplastic to hypertrophic growth. During embryonic development in mammals, cardiomyocytes actively proliferate to build a functional heart, a phenomenon known as hyperplastic growth. Subsequently, during the early postnatal development, coincident with the first week of postnatal life in mice, most cardiomyocytes withdraw from the cell cycle and continue to grow in size (hypertrophic growth) [15,16]. The evidence of the increase in GR abundance in cardiomyocytes during the early postnatal period (see **Fig. 2**), along with the robust inhibitory activity of GCs/GR axis on neonatal cardiomyocyte proliferation (see **Figs. 1-3**) prompted us to investigate a potential cardiomyocyte intrinsic role for GR in the physiological cardiomyocyte maturation and transition from hyperplastic to hypertrophic growth occurring shortly after birth.

As a first indication of cardiac growth upon cardiomyocyte-specific GR ablation, we measured the heart weight normalized to body weight (HW:BW ratio) of GR-cKO compared to control mice. At postnatal day 7 (P7) a modest increase in HW:BW ratio was observed in GR-cKO (**Fig. 4a**). GR-cKO cardiomyocytes displayed reduced size (**Fig. 4b**), without significant differences in markers of cardiac pathological hypertrophy (**Extended Data Fig. 3b**). Importantly, stereological analysis demonstrated an increase in the total number of cardiomyocytes in GR-cKO hearts compared to controls (**Fig. 4c**). Further, immunofluorescence analysis revealed an augmented proliferation of cardiomyocytes in P7 GR-cKO hearts compared to controls (**Figs. 4d-e**). In line, the ratio of mono- to bi-nucleated cardiomyocytes was increased in P7 GR-cKO compared with control cultures (**Fig. 4f**).

These results show that the *in vivo* deletion of GR prolongs the postnatal proliferative window of cardiomyocytes while reducing the hypertrophic growth and binucleation, suggesting a role for GR in postnatal cardiomyocyte maturation (**Fig. 4g**).

GR-cKO delays the postnatal maturation of cardiomyocyte myofibrils-mitochondria organization.

During the early postnatal development, the cytoarchitectural structure of cardiomyocytes undergoes maturation, shifting from loose spatial organization to highly organized and efficient contractile units [39,40]. Confocal microscopy of heart sections from P7 GR-cKO compared to control mouse model unveiled the presence of reduced and partially disassembled myofibrils, as detected by the striation pattern (**Extended Data Fig. 3c**). Next, we performed ultrastructure analysis by transmission electron microscopy (TEM) of GR-cKO and control cardiomyocytes at birth and during the early postnatal development. As already documented in the literature, neonatal (P1) cardiomyocytes displayed an immature myofibrillar organization with chaotically arranged myofibrils, and large free cytoplasmic space between myofibrils and isolated mitochondria (**Extended Data Figs. 3d-e)**. Neonatal GR-cKO cardiomyocytes appeared slightly more immature, as visible by fewer and randomly organized myofibrils (**Extended Data Figs. 3f-g)**. These data support previous studies suggesting a role of GR in foetal cardiomyocyte maturation during late gestation [24–26]. During early postnatal development, a profound maturation of cardiomyocyte cytoarchitecture occurs. This process is coupled with the emergence of organized mitochondrial networks allowing the formation of energy micro-domains, which are responsible for the efficient energy transfer system from mitochondria to sarcomere structures [40]. In line, compared to neonatal (P1) stage, postnatal day 7 (P7) control cardiomyocytes had substantially reduced free cytoplasmic space, with aligned and organized myofibrils in close contact with clustered mitochondria (**Fig. 5a,** mitochondria magnification in **Fig. 5b**). Myofibrils appeared regularly and parallely oriented with normal Z line banding (**Fig. 5c**). However, at this stage, GR-cKO cardiomyocytes appear immature, with a high content of free cytoplasm and an irregular and misaligned pattern of myofibrils with loss of the major axis orientation and arrangement around isolated mitochondria (**Fig. 5d,** mitochondria magnification in **Fig. 5e**). Of note, GR-cKO hearts showed accumulation of lipid droplets (see **Fig. 5d**). Finally, the sarcomere apparatus in GR-cKO cardiomyocytes featured a poor A, I, H bands and M organization (**Fig. 5f**). To

sum up, GR-cKO mice develop a delay in myofibrils-mitochondria organization, which at postnatal day 7 resembles the organization of neonatal cells. These results suggest that GR concurs to the physiological maturation of myofibrils-mitochondria organization occurring in cardiomyocytes during the early postnatal period (**Fig. 5g**).

GR-cKO increases cardiomyocyte proliferation by favouring glucose catabolism over fatty acid oxidation.

In order to uncover the mechanism by which GR contributes to cardiomyocyte maturation and cell cycle exit, we performed RNA-sequencing analysis of neonatal (P1) GR-cKO and control cardiomyocyte cultures. Gene ontology analysis of these data highlighted significant differences in metabolic processes, in particular regarding the glycolytic process (**Fig. 6a**). Interestingly, the heatmap of glycolytic genes uncovered that GR-cKO heart cell cultures have increased expression levels of enzymes in every step of the glycolytic cascade, which converts glucose to pyruvate (**Fig. 6b**). Beginning in late gestation and continuing through the first weeks after birth in the mouse model, cardiomyocytes undergo an important rewiring from glucose catabolism to oxidative metabolism in mitochondria dependent on lipid utilization [40,41]. Human cardiomyocyte maturation has also been associated with transcriptional activation and gain of accessibility around the promoters of genes involved in regulation of the transition from glycolysis towards fatty acid catabolism [42]. This transition is required for the establishment of an efficient energy production system to face the substantial increase in cardiac workload consequent to the organism's growth [40]. We therefore performed RNA-sequencing analysis of P7 GR-cKO and control hearts. As expected, GR was among the most significantly down-regulated genes in GR-cKO hearts (**Extended Data Fig. 3h**). In the same short list of regulated genes, we noticed the increased expression of Acta2, which has been suggested as a marker for cardiomyocyte immaturity/dedifferentiation together with Runx1, Dab2 and cKit [43,44]. By checking the expression of these markers, we observed a statistically significant upregulation of Runx1 in GR-cKO heart lysates (**Extended Data Fig. 3i**), which was confirmed in cardiomyocytes in heart sections (**Extended Data Fig. 3j**), further supporting the role of GR in promoting cardiomyocyte maturation during the early postnatal development. Interestingly, gene ontology analysis according to biological processes highlighted major changes in gene networks linked to NADP, lipids, and ATP metabolism (**Fig. 6c, Extended Data Figs. 4a-b**). Specifically, GR-cKO hearts displayed increased

expression of several enzymes involved in metabolism of NADPH (**Fig. 6d)**, including some genes (*Pgls* and *Tkt*) of the pentose phosphate pathway, which produces five-carbon sugars (pentoses) for nucleotide biosynthesis and directs pentoses towards glycolysis. Further, the expression of several genes promoting fatty acid oxidation was significantly reduced in GR-cKO hearts, including *Pdk4* (**Fig. 6e**). Moreover, a general reduction in expression levels of several subunits of the respiratory complexes I (*mt-Nd4*), II (*Sdhc*), III (*Uqcrfs1* and *mt-cytB*), IV (*Cox7c*), cytochrome c (*Cycs*) and enzymes responsible for the transfer of energy from mitochondria to the cytosolic carrier creatine was observed in GR-cKO hearts (**Fig. 6f, Extended Data Figs. 4c-d)**. Overall, these data suggest that GR reduces the expression of genes involved in glucose catabolism while increasing those involved in fatty acid oxidation, mitochondrial respiration and energy transfer from mitochondria to the cytosol (**Extended Data Fig. 5)**.

Notably, the transition from glycolysis to fatty acid oxidation coupled with the increase in mitochondrial oxidative metabolism, has been shown to represent a key factor in the loss of cardiomyocyte proliferative and regenerative ability [45–49]. Based on RNA-sequencing data, we thus decided to focus our investigations on mitochondrial respiration and glycolysis by measuring oxygen consumption rate (OCR) and extracellular acidification rate (ECAR) in cardiomyocytes isolated from control and GR-cKO mice, under basal conditions or following inhibition of fatty acid oxidation or glycolysis. These experiments intended to investigate the contribution of metabolic ways in feeding the respiratory chain. Overall, no overt differences in oxygen consumption rate profiles were observed between GR-cKO cardiomyocytes and controls (**Fig. 6g)**. Basal respiration and maximal respiration capacity were not affected by GR deletion **(Extended Data Figs. 6a-b)** as well as extracellular acidification rate **(Extended Data Fig. 6c)**. In line, the activities of respiratory complexes were comparable between controls and GR-cKO hearts (**Extended Data Fig. 6d**). These data suggest that the lack of GR does not induce an evident mitochondrial respiratory defect. However, GR-cKO heart cell cultures compared to controls showed a modest reduction in the spare respiratory capacity, i.e. the difference between maximal respiration and basal respiration **(Fig. 6h)**, suggesting a reduced ability to respond to increasing energy demand. Next, we evaluated the contribution of long chain fatty acid oxidation to oxygen consumption rate, by inhibiting fatty acid oxidation with etomoxir, which acts through its irreversible inhibitory effects on the carnitine palmitoyl-transferase 1a

(CPT1a). Upon addition of etomoxir, GR-cKO cardiomyocytes showed a reduced acute response compared to controls, suggesting that these cells are less dependent on fatty acid oxidation for their mitochondrial respiration **(Fig. 6i and Extended Data Figs. 6e-g)**. In this frame, it can be hypothesized that the reduced use of lipids to fuel respiration may induce their storage, consistent with accumulation of lipid droplets observed in P7 GR-cKO hearts (see **Fig. 5d**). Importantly, the assessment of the proliferation of cardiomyocytes isolated from control and GR-cKO neonatal hearts upon the administration of 2-deoxy-glucose (2dG), a glucose mimic that inhibits glycolysis and the pentose phosphate pathway, unveiled that inhibition of glucose catabolism reduces the proliferation of GR-cKO cardiomyocytes, while having no significant impact on the proliferation rate of control cardiomyocytes (**Fig. 6j**). We also analysed cellular respiration in response to the administration of 2dG. As expected, inhibition of glucose catabolism in control cardiomyocytes resulted in a modest reduction in maximal respiration (**Extended Data Fig. 6h**), in line with a modest dependence on glucose catabolism in control cardiomyocytes. Conversely, inhibition of glucose oxidation in GR-cKO cardiomyocytes paradoxically increased maximal oxygen consumption rate (FCCP administration in **Extended Data Figs. 6i-j**). Upon 2dG injection no differences in acute response were observed (**Extended Data Fig. 6k**), but both maximal respiration and spare respiratory capacity were increased in GR-cKO cardiomyocytes compared to controls (**Extended Data Figs. 6l-m**), possibly due to an increased ability of GR-cKO cardiomyocytes to switch between different energetic sources to sustain cellular respiration.

Next, we crossed the list of metabolic genes modulated in GR-cKO mice (**see Figs. 6b,d-f**) with a validated list of GR target genes, activated by the synthetic agonist dexamethasone by direct binding of GR to their promoters [50]. This analysis unveiled the pyruvate dehydrogenase kinase 4 (*Pdk4*) as the only GR directly induced gene in our list. *Pdk4* was also among the set of genes that emerged from the integrated analysis of GR targets genes [50] showing significant upregulation during early postnatal development [51] (**Extended Data Fig. 7**). Importantly, Pdk4 is a key player in the postnatal transition from glucose catabolism to fatty acid oxidation, and its deletion has been recently proven to be sufficient to increase cardiomyocyte proliferation and cardiac regeneration following myocardial infarction [47].

Overall, these data suggest that, in the early postnatal period, active GR signalling favours fatty acid oxidation over glucose catabolism for cardiomyocytes' energetic

function, a transition that is associated with cardiomyocyte maturation and cell cycle exit.

GR-cKO promotes cardiomyocyte regeneration after myocardial infarction.

All the data collected so far strongly supported a role of GCs/GR axis in promoting cardiomyocyte maturation, while restraining proliferation, during the early postnatal development. Next, we tested whether GR ablation is sufficient to promote cardiomyocyte proliferation upon myocardial injury. To this end, we induced myocardial infarction (MI) by permanent ligation of the left anterior descending coronary artery in GR-cKO and control mice at P7 stage, when the majority of cardiomyocytes have already exited from the cell cycle, and we evaluated cardiomyocyte proliferation 10 days post-MI (**Fig. 7a**). Cardiomyocyte cell cycle re-entry was increased both in remote and border zones of myocardial infarction in GR-cKO mice (**Fig. 7b**). Furthermore, the level of cycling cardiomyocytes with marginalization of sarcomere structures to the cell periphery was robustly increased in GR-cKO hearts compared to controls (**Fig. 7c)**. This phenomenon has been documented during the spontaneous regeneration process following cardiac injury in neonatal mice and it is considered as a prerequisite to effective cardiomyocyte division [1,6]. Moreover, Aurora B positive cardiomyocytes were increased in GR-cKO hearts (**Fig. 7d**). These data, therefore, suggest that GR-cKO cardiomyocytes after myocardial infarction are more prone to disassemble the sarcomere components to undergo successful cell division. Finally, we decided to analyse if GR deletion is sufficient to induce cardiomyocyte proliferation at adult stage. Surprisingly, in absence of damage, 2 months-old GR-cKO mice showed no significant differences in cardiomyocyte cell cycle activity compared to controls (**Fig. 7e**). To evaluate the effect of GR ablation in the adult heart after damage, we performed MI in GR-cKO and control adult (~3-months old) mice and analysed the hearts at multiple time points post-MI, acutely and chronically (**Fig. 7f**). First, we evaluated a putative cardioprotective effect of GR ablation by performing triphenyltetrazolium chloride (TTC) staining in GR-cKO versus control mice soon after the MI (about 24 hours). Interestingly, a significant reduction in damage extensions was observed in GR-cKO mice, suggesting that the ablation of GR exerts an immediate cardioprotective role (**Fig. 7g**). Further, 11 days post-MI, cardiomyocyte proliferation was increased in GR-cKO compared to control adult hearts, both in the border and remote zones (**Fig. 7h**). Finally, 30 days post-MI, while

cardiomyocyte proliferation in control mice returned back to the levels of uninjured mice, it remained slightly increased in the border zone of GR-cKO hearts (**Fig. 7i**). In addition, 30 days after MI, GR-cKO adult hearts displayed reduced scarring along with an increase in healthy muscular tissue (**Fig. 7j**), and an overall improvement in cardiac performance (**Fig. 7k**), as evidenced by echocardiographic analysis. Altogether, these data demonstrate that the deletion of GR induces cardiomyocyte survival and facilitates cell cycle re-entry and proliferation upon cardiac injury, resulting in tissue regeneration with reduced scar formation.

Transient GR inhibition promotes cardiomyocyte regeneration after myocardial infarction.

Previous analyses, performed in ~4-months-old mice, reported that the lack of GR in the long term is detrimental for heart function [38], which we also documented (**Extended Data Fig. 8**). We thus decided to test the feasibility of a transient approach. To test whether transient pharmacologic antagonization of GR may represent a therapeutic strategy to enhance cardiomyocyte proliferation and cardiac regeneration in the adult mammalian heart, avoiding detrimental effects, we first evaluated if the negative effect exerted by corticosterone on cardiomyocyte proliferation is permanent or transient. To address this issue, cultured cardiomyocytes were treated with corticosterone for 24 hours and then DNA synthesis was assessed by BrdU incorporation immediately or after 24 or 48 hours of corticosterone wash-out with normal medium. Interestingly, the data suggest that the suppressive effect of corticosterone on cardiomyocyte proliferation is transient, lasting between 24 and 48 hours (**Fig. 8a**).

We then analysed the effect of transient GR antagonization on cardiac regeneration by delivering the GR antagonist Mifepristone (RU486) in animals subjected to MI (as schematized in **Fig. 8b**). MI was induced in 3 months-old mice and RU486 was delivered to animals for 14 days, starting immediately after the induction of the infarction. Mice were either sacrificed at the end of the treatment to evaluate cardiomyocyte proliferation (14 days post-MI), or 3 weeks later (35 days post-MI) to evaluate the scar size and heart functionality. The administration of RU486 elicited a robust and transient increase in the number of proliferating cardiomyocytes in the hearts of adult mice subjected to MI, as assessed through the analysis of Ki67 and Aurora B markers at the end of the RU486 administration window (2 weeks post-MI) and 3 weeks later **(Figs. 8c-e)**. The hearts of RU486 treated animals, 5 weeks after the induction of

MI, showed a reduction in the scar size, along with an increase in the percentage of healthy tissue (**Fig. 8f**) and a partial recovery of heart functionality (**Fig. 8g**).

Altogether, these results suggest that a transient inhibition of GR promotes cardiomyocyte proliferation and heart regeneration after MI in the adult mammalian heart, introducing GR in the small cohort of promising druggable targets to increase adult mammalian heart regeneration capacity after myocardial injury.

DISCUSSION

In the last few years, the role of glucocorticoid signalling in cardiomyocytes is receiving increased attention [24,25]. In this study, we unveiled the physiological role of endogenous glucocorticoids (GCs) and their receptor GR in promoting postnatal cardiomyocyte cytoarchitectural maturation and cell cycle exit in the early postnatal period. In line with our study, GCs were also shown to enhance T-tubule development and mature excitation–contraction coupling of human IPS-derived cardiomyocytes,[52] and human cardiomyocyte maturation was recently shown to be associated with a gain of accessibility around GR binding sites [42]. Of note, the physiological role of GR in repressing cardiomyocyte proliferation, in line with a recent study [31], might appear in contrast with the reported promotion of cardiomyocyte proliferation induced by glucocorticoids during prenatal stages, which has been shown to be mediated by the cognate receptor MR [27,28]. Further studies are therefore required to evaluate if a glucocorticoid-induced MR activation contributes to the increased cardiomyocyte proliferation observed after GR ablation or antagonization. The role of MR and its relationship with GR in heart health and disease are emerging [24,25] and deserve further investigations in the context of postnatal cardiomyocyte proliferative and regenerative ability.

Quite surprisingly, at adult stage, we did not observe significant differences in cardiomyocyte proliferation in GR-cKO mice compared to controls. Consistently, no *in vivo* differences were recently reported in GR-cKO mice at postnatal day 14 [31], an observation that probably discouraged further investigations on the potential role for GR in regulating the cardiomyocyte proliferative potential loss. Nevertheless, we unveiled that GR ablation, upon cardiac injury, in adult mice facilitates cardiomyocyte cell cycle re-entry, sarcomere disassembly and cell division, thus promoting cardiac regeneration along with reduced scar formation and improved muscle tissue replacement. Our study therefore suggests that GR acts as a molecular brake for

cardiomyocyte proliferative and regenerative signalling pathways activated in response to cardiac damage.

The long term absence of GR has been reported detrimental for heart function [38]. Importantly, transient GR inactivation by the delivery of RU486 was sufficient to promote cardiac regeneration circumventing issues related to chronic GR inhibition, thus representing a potential therapeutic approach for myocardial injuries in patients. RU486 is a drug already approved for clinical use and with non-serious side effects, therefore we speculate that its transient use following heart attack would be promising. Nevertheless, other GR inhibiting strategies deserve further investigations in the context of cardiac regeneration, for example based on drugs that inhibit glucocorticoids production (inhibitors of steroid 11-beta-monooxygenase) or more specific GR modulators.

Intriguingly, our data suggest that GR limits cardiomyocyte proliferative ability, at least in part by regulating genes involved in metabolic rewiring from glucose catabolism to fatty acid oxidation for mitochondrial respiration. In this frame, our functional data indicates GR signalling cascade as an important player in controlling the fuelling of mitochondrial respiration during cardiomyocyte maturation. Nevertheless, our conclusions in this regard rely only on gene expression analysis and measurements of metabolic respiration, highlighting the need of a more detailed investigation of metabolic fluxes by mass spectrometry combined with gas chromatography (GC) or liquid chromatography (LC), the gold standard for the precise definition of metabolic settings and flexibility, which was not performed in the current study due to technical limitations.

Importantly, cellular energy metabolism and mitochondrial respiration have recently emerged as important regulators of differentiation, proliferation and regeneration of endogenous cardiomyocytes [3,41,45–49,53]. Indeed, during the early postnatal period, the increase in oxygen levels and oxidative energetic mitochondrial metabolism along with the metabolic shift from a glucose-based metabolism to an energetic production mostly relying on fatty acid oxidation have been shown to contribute to the decline in heart regenerative ability [45,47].

Overall, our data appears broadly consistent with emerging reports suggesting that cardiac regenerative capacity in mammals is controlled by a developmental switch in metabolic pathways that are governed by nuclear hormone receptor signalling pathways, downstream to glucocorticoid receptor, androgen receptor, progesterone receptor, and

thyroid hormone receptor. Indeed, in addition to GR, Androgen Receptor (AR) and Progesterone Receptor (PR) were also recently suggested to play a role in human cardiomyocyte maturation [42]. In particular, PR plays a role in determining cardiomyocyte contractility and maturation in both males and females, with the establishment of sex-specific transcriptional programs associated with fatty acid oxidation, lipid metabolism, tricarboxylic acid cycle, and respiratory electron transport chain [42]. The thyroid hormone receptor was recently demonstrated to play a role in IPS-derived cardiomyocytes [52], as well as in the regulation of cardiac regenerative capacity in mice with a suggested mechanism involving alterations in cardiac metabolism [54].
In summary, our study unveils an important role for GCs/GR axis in cardiomyocyte maturation and cell cycle exit during the early postnatal development and in restraining their regeneration potential in juvenile and adult stages (**Extended Data Fig. 9**). We suggest GR antagonization as a promising approach for heart regeneration based on endogenous cardiomyocyte renewal.

METHODS

Animal studies. All animal procedures were approved and performed in accordance with the Institutional Animal Care and Use Committee of University of Bologna (Bologna, Italy), Cogentech/IFOM (Milan, Italy), King's College London (London, United Kingdom), ICGEB (Trieste, Italy) and Weizmann Institute of Science (Rehovot, Israel). Mice were housed at a controlled temperature of 20-25 °C and a relative humidity of 40-60%, following a 12h:12h light:dark cycle.
Mice studies were performed on C57BL/6 background, with the exception of cardiomyocyte-specific GR knock-out (GR-cKO) mice, which were generated by mating animals expressing Cre under the promoter of Myh6 (Myh6-Cre mice, FVB/N x C57BL/6 background) with animals harbouring loxP sites flanking the exon 3 and 4 of GR gene ($GR^{flox/flox}$ mice, 129 x C57BL/6 background)(see **Fig. 3a**). Oligonucleotide sequences for genotyping the above-described mouse lines are listed in **Supplementary Table 1**. Mice age is reported in the main text, figures and/or figure legends. Data were aggregated without discriminating for gender.

Cardiac cell isolation and culture. For isolation of P1 primary cardiac cells, hearts were harvested from 1-day-old (P1) mice and were subjected to multiple enzymatic digestions with pancreatin and collagenase, performed under agitation at 37°C. For

isolation of P7 primary cardiac cells, hearts were harvested from 7-day-old (P7) mice and subjected to clamping of the aorta and antegrade perfusion with an enzymatic solution containing $CaCl_2$, collagenase, trypsin and protease, followed by incubation in a solution with 0,2 % BSA and 1,2 mM $CaCl_2$ at 37°C. The cardiac cells were then cultured in gelatine-coated (0.1%, G1393, Sigma) wells with DMEM/F12 (Aurogene) supplemented with L-glutamine, sodium pyruvate, non-essential amino acids, penicillin, streptomycin, 5% horse serum (HS) and 10% foetal bovine serum (FBS) (hereafter referred to as 'complete-medium') at 37°C and 5% CO_2. The cardiac cells were allowed to adhere for 48 hours in complete-medium. Subsequently, the medium was replaced with an FBS-deprived complete-medium containing Corticosterone (27840, Sigma), Mifepristone (RU486, M8046, Sigma) or Eplerenone (E6657, Sigma) at the indicated concentrations for 48 hours. For BrdU assay, BrdU (10 µM, B5002, Sigma) was introduced along with the treatments.

Cardiomyocyte and stromal cell separation. To assess proliferation or the differential gene expression in cardiomyocytes and cardiac stromal cells in P1 and P7 hearts, we proceeded as follows. P1 hearts were subjected to enzymatic digestion as described above, whereas P7 hearts were harvested and anterogradely perfused with digestion enzymes (collagenase, trypsin, protease). Cardiomyocytes were separated from stromal cells using the immuno-magnetic cell sorting MACS Neonatal Isolation System (130-100-825, Miltenyi biotech), following the manufacturer's protocol. The different cells were then cultured as described above or centrifuged and subjected to total RNA extraction from the pellet as described below.

Immunofluorescence on cells and tissue sections. Cultured cells were fixed with paraformaldehyde (PFA) 4% (Sigma, diluted in Phosphate Buffered Saline (PBS) for 20 minutes at 4°C. Heart sections underwent deparaffinization (by immersion in Xylene and rehydration by immersion in solutions with a decreasing concentration of Ethanol), and heat-induced antigen retrieval in a sodium citrate solution (Sigma) at pH 6.0, followed by gradual chilling. Then heart sections and cultured cells were processed in the following manner. Samples were permeabilized with 0.5% Triton-X100 (Sigma) in PBS for 5 minutes at room temperature and the non-specific binding of the antibodies was prevented by applying a blocking solution of 5% BSA (Sigma) and 0.1% Triton-X100 in PBS for 1 hour at room temperature. For the BrdU staining protocol, a DNA

hydrolysis step between the permeabilization and the blocking step was performed by the addition of 2M HCL (Sigma) for 30 minutes at 37°C and then 3 washes in PBS.
Then samples were incubated overnight at 4° C with the following antibodies diluted in PBS supplemented with 3% BSA and 0.1% Triton-X100. Anti-cTnT (1:200, ab33589, Abcam) and anti-cTnI (1:200, ab47003, Abcam) antibodies were used to identify cardiomyocytes. Anti-Ki67 antibody (1:50, ab16667, Abcam), anti-BRDU antibody (1:40, G3G4, DSHB), and anti-aurora B (1:50, 611082, BD Transduction Laboratories) antibodies were used to analyse cell cycle re-entry, DNA synthesis and cytokinesis, respectively. Other antibodies and dyes used in the study: anti-GR (1:50, 12041S, Cell Signalling), wheat germ agglutinin (WGA) AlexaFluor488-conjugated (1:200, Invitrogen, 29022-1).
After primary antibody incubation, 3 washes in PBS were performed and samples were incubated for 1 hour at room temperature with fluorescent secondary antibodies, diluted in PBS supplemented with 1% BSA and 0.1% Triton-X100. Secondary antibodies used: anti-mouse AlexaFluor 488 (115-545-003, Jackson), anti-rabbit AlexaFluor 488 (111-545-003, Jackson), anti-mouse Cy3 (115-165-003, Jackson), anti-rabbit 594 (AlexaFluor 111-585-003, Jackson).
After 3 washes in PBS, DAPI (4',6-diamidino-2-phenylindole dihydrochloride, Sigma), diluted in PBS, was applied for 15 minutes at room temperature for nuclei visualization. Samples were then washed 2 more times in PBS. Cells in culture plates were imaged at the Zeiss Axio Observer A1 microscope by Volocity 6.3.1 software or at the ThermoFisher ArrayScan XTI microscope by ArrayScan HCS Studio 6.6.0 software. Slides were mounted with an antifade solution (Vectorlabs), covered with a coverslip, sealed with nail polish and imaged at the Zeiss Axio Observer A1 microscope by Volocity 6.3.1 software, at the Nikon Eclipse 80i and Nikon Eclipse TI2 fluorescence microscope by Nis Elements 5.21 software, at the Olympus vs200 Slide Scanner by software vs200 ASW 3.1, and at a Leica TCS SP5 confocal microscope by LAS AF 2.7.3 confocal software.

Time-lapse videos. 48 hours after seeding, P1 primary CMs were exposed to 10nM TMRE (tetramethylrhodamine ethyl ester, Sigma), diluted in serum free medium, for 20 minutes at 37°C. TMRE is a fluorescent dye that labels mitochondria, used to selectively label cardiomyocytes [33]. Live-cell imaging was performed using a widefield

fluorescent microscope (Nikon Eclipse TI2). Time-lapse imaging was carried out for 16 h and images were acquired at ×40 magnification every 15 minutes.

Assessment of cardiomyocyte size. The cross-sectional area of cardiomyocytes in P7 hearts was assessed using ImageJ 1.52p software (National Institutes of Health) on the basis of wheat germ agglutinin (WGA) staining. For that purpose, slides were deparaffinized as described above, rinsed in PBS and then incubated overnight at 4°C with WGA conjugated to Alexa Fluor 488 (1:200, Invitrogen, 29022-1). Slides were then rinsed 3 times in PBS, mounted with an antifade solution (Vectorlabs) and imaged at a widefield microscope (Nikon Eclipse 80i). Only cardiomyocytes that were aligned transversely were considered for the quantification of the cross-sectional area.

Assessment of cardiomyocyte number in juvenile mice. Heart weight was multiplied by the known value for the specific gravity of muscle tissue (1.06 g/ml) to obtain heart volume. The calculated heart volume was multiplied by the fraction occupied by cardiomyocytes (calculated in heart sections on the basis of cTnT staining) to determine the total volume of cardiomyocytes. Average cardiomyocyte volume was calculated utilizing measurements from cardiomyocyte cross-sectional areas multiplied by the average of cardiomyocyte lengths (see 'Assessment of cardiomyocyte size' above). The number of cardiomyocytes per heart was calculated as the quotient of the total volume of cardiomyocytes and average cardiomyocyte volume.

Transcriptional analysis. Total RNA extraction was performed with NucleoSpin RNA II kit (Macherey Nagel) according to the manufacturer's protocol. RNA quantification and quality check were performed using a Nanodrop spectrophotometer (N1000, Thermo). RNA was reverse transcribed to cDNA with VILO (Thermo Fisher) according to the manufacture's protocol. Real Time (rt)-PCR was performed using Fast SYBR Green PCR Master Mix (Applied Biosystems) on a QuantStudio 6 Flex instrument (Applied Biosystems). Data were collected with QuantStudio RealTime PCR software 1.3 (Applied Biosystems). Oligonucleotide sequences for real-time PCR analysis performed in this study are listed in **Supplementary Table 2**.

RNA sequencing. Transcriptomic analysis was performed using QuantSeq FWD 3' mRNA-Seq Services of Lexogen. Briefly, purified total RNA was extracted from *in*

vitro cultures of cardiomyocytes and from whole heart homogenates; single read sequencing was performed on NextSeq 500 (Illumina) and quantification was based on tags in 3' region with more than 20M reads per sample. The data analysis was performed with the following softwares: NextSeq Control Software v2.2.0.4 (for base-calling), BCL to FASTQ file converter bcl2fastq (for demultiplexing), cutadapt v1.16 (for trimming), FastQC v0.11.7, multiqc v1.5, STAR v2.5.4a (for alignment), featureCounts v1.6.2 (for counting), DESeq2 v1.18.1 (for differential expression). Enriched GO term analysis and heatmaps were performed using *goseq* and *heatmap2* Galaxy packages. Heat maps in **Fig. 6** as well as in **Extended Data Fig. 4** include all statistically significant genes belonging to a specific gene ontology term. The list of genes included in each gene ontology was downloaded from Mouse Genome Informatics website (http://www.informatics.jax.org/vocab/gene_ontology/). Gene ontology terms were selected among those showing a statistically significant enrichment in GR-cKO compared to ctrl heart lysates or cell cultures, as specified in the figure legend.

Protein extraction and Western Blotting. Western blotting was performed with the SDS–PAGE Electrophoresis System. Proteins were extracted with RIPA buffer with the addition of proteinase inhibitor (Sigma) and phosphatase inhibitors (cocktail 2 and 3, Sigma). SDS-PAGE was performed with 45 μg of protein extracts and transferred to PVDF membrane, which was then incubated with the following antibodies: anti-GR (1:1000, 12041S, Cell Signalling) and anti-Actin B (1:100, sc-47778, Santa Cruz). Horseradish peroxidase (HRP) conjugated anti-rabbit antibody (1:200, NA934, GE) was used as secondary antibody. Signals and images were acquired by Chemi Doc™ XRS 2015 (Bio-Rad), with ECL substrate (Clarity Western ECL Substrate, Bio-Rad).

Assessment of serum corticosterone levels through ELISA assay. Blood samples were collected by decapitation for early postnatal mice (at P1, P3, P5, P7 stages) and by cardiac puncture for juvenile mice (at P14, P28 and P56 stages). Subsequently, samples were centrifuged at 2000 g for 10 minutes, for serum fraction collection. The quantification of serum levels of circulating corticosterone was performed using an ELISA kit (ADI-900-097, Enzo Life Sciences) according to the manufacturer's instructions. Absorbance was measured at 405 nm using a Tecan Spark multifunctional

microplate reader. Concentrations for each sample were determined as the percentage bound using a standard curve with detection range between 20000 and 32 pg/ml.

Electron Microscopy. Small myocardial samples were fixed after surgery in 2.5% glutaraldehyde in 0.1 M cacodylate buffer at pH 7.4 and postfixed in 1% OsO_4 in the same buffer. After dehydration in graded ethanol specimens were embedded in Araldite. Thin sections were stained in uranyl acetate and lead citrate and imaged with Philips CM10 Transmission Electron Microscope and iTEM FEI 5.2 software.

Mitochondria isolation and respiratory complexes activity. Crude mitochondria were used to assess respiratory chain enzymatic activities. Three entire hearts with the same genotype were pooled and homogenized in ice-cold Sucrose-Mannitol Buffer (220 mM mannitol, 75 mM sucrose, 1 mM EGTA and 10 mM Tris-HCl, 0.1% BSA, pH 7.4) and homogenized first with TissueRuptor II (Qiagen) and then with a glass/teflon Potter homogenizer. The obtained samples were centrifuged at 1500 g for 50 min at 4 °C to discard unbroken cells, tissue fragments and nuclei. The resulting supernatant was centrifuged at 10000 g for 10 min at 4 °C to separate crude mitochondria from the remaining sub-cellular fractions of the sample. Mitochondria were stored at -80°C in aliquots for subsequent investigations. CI (NADH:DB:DCIP oxidoreductase), CI+CIII (NADH:cytochrome *c* reductase), CII (succinate/DCPIP), CII+CIII (succinate:cytochrome *c* reductase), CIII (cytochrome *c*/DBH_2), and CIV (cytochrome *c* oxidase) activities were measured at 37°C by using a dual-wavelength spectrophotometer (V550 Jasco Europe, Italy). Respiratory chain complexes specific activity was normalized to protein content (quantified by NanoDrop 2000, ThermoFisher Scientific) and citrate synthase (DTNB:oxaloacetate) activity.

Microrespirometry assay. Mitochondrial oxygen consumption rate (OCR) and extracellular acidification rate (ECAR) respiration were evaluated using the Seahorse Xfe Substrate Oxidation Stress Test protocols. Cells were seeded (17×10^3 cells/well) in 70 µL of complete-medium into gelatinized Xfe96 cell culture plate and allowed to attach for 48 h. Cell culture media was replaced with 180 µL Seahorse XF DMEM Medium supplemented with 10 mM glucose, pH 7.4 (Agilent #103575-100, XF-medium). OCR and ECAR were measured over a 3 min period, followed by 3 min of mixing and re-oxygenation of the medium. Cells were incubated at 37 °C for 30 min to

allow temperature and pH equilibration. After three OCR basal measurement (basal respiration), an injection of either 20 µL of XF-medium, 5µM 2dG or 40 µM etomoxir was performed followed by six measurements. Then, OCR was measured upon sequentially injections of 1 µM oligomycin, 1 µM carbonyl cyanide-p-trifluoromethoxyphenylhydrazone (FCCP), and 0.5 µM rotenone plus 0.5 µM antimycin A. Three measurements of OCR were obtained following injection of each drug. Basal respiration was calculated by subtracting non-mitochondrial respiration from baseline OCR; after addition of oligomycin, a complex V inhibitor, OCR was used to calculate ATP-linked respiration (by subtracting the oligomycin rate from baseline OCR) and proton leak respiration (by subtracting non-mitochondrial respiration from the oligomycin OCR); Carbonyl cyanide-p-trifluoromethoxyphenylhydrazone (FCCP) was added to uncouple oxidative phosphorylation pushing the electron transfer chain to function at its maximal rate, and maximal respiratory capacity was derived by subtracting non-mitochondrial respiration from the FCCP OCR; antimycin A and rotenone, inhibitors of complex III and I respectively, were added to measure non-mitochondrial oxygen consumption. At the end of each experiment, the medium was removed and sulforhodamine B (SRB) assay was performed to determine the amount of total cell proteins. Raw OCR and ECAR data were normalized to total protein levels (SRB protein assay) in each well and analysed using Wave Controller 2.6 Seahorse Analytics software (https://seahorseanalytics.agilent.com/). Acute response is calculated as the difference in OCR after injection of either 2dG or etomoxir and XF-medium.

***In vivo* drug delivery.** In the experiment analysing the effects of GR blockage during physiologic postnatal development, GR antagonist Mifepristone (RU486, Sigma M8046) was dissolved in the drinking water (42 µg/ml, equivalent to 20 mg/kg/day) and administered *ad libitum* to the lactating mother, starting from the day of the birth of the pups and continuing the treatment for 7 days, and replacing every day the solution with a freshly prepared one. Based on previous studies [55] the amount of RU486 received by pups is expected to be around 0.3mg/kg. In the experiment analysing the effects of GR blockage after myocardial infarction in adulthood, GR antagonist Mifepristone (RU486, Sigma M8046) was delivered through the food (special food diet dry pellets

were produced by a commercial manufacturer, Mucedola), with a dose of 20 mg/kg/day, starting the administration immediately after the myocardial infarction procedure.

Myocardial infarction. Myocardial infarction at juvenile (P7) or adult stage was induced by ligation of the left anterior descending coronary artery. P7 mice were anaesthetized by cooling on an ice bed for 4 min, whereas adult mice were sedated with isoflurane (Abbott Laboratories) and, following tracheal intubation, were artificially ventilated. Lateral thoracotomy at the fourth intercostal space was performed by blunt dissection of the intercostal muscles following skin incision. Following ligation of the left anterior descending coronary artery, thoracic wall incisions were sutured with 6.0 non-absorbable silk sutures, and the skin wound closed using skin adhesive. Mice were then warmed for several minutes until recovery. The decline in heart function was verified 1 or 2 days post-MI and mice with similar myocardial function were further analysed at different time points, as specified in the main text and figures.

Echocardiography. Heart function was evaluated by transthoracic echocardiography performed on sedated mice (isoflurane, Abbott Laboratories) using a Vevo 3100® device and Vevo Lab 3.2.6 software (VisualSonics) or MyLab 70 XV device.

Histology (Masson's trichrome). Murine hearts were fixed in 4% PFA for 24 hours, then embedded in paraffin, sectioned (3μm thick) with a microtome (Leica) and attached to SuperFrost II plus slides (Thermo). For analysis of cardiac regeneration following the myocardial infarction procedure, paraffin sections were cut through the entire ventricle from apex to base into serial sections. Masson's trichrome staining was used for the detection of fibrosis and performed with a standard kit (Bio-Optica, 04-010802A) according to the manufacturer's protocol. Scar size was quantified in each section with ImageJ 1.52p software (National Institutes of Health) based on Masson's trichrome staining. The percentage of myocardial tissue volume occupied by scar was calculated as the sum of scar volumes between serial sections normalized on the total left ventricular and septal tissue volume. The volume between serial sections was calculated with the formula of a truncated pyramid: $\frac{1}{3}\ \mathbf{i}\ (\boldsymbol{a1} + \boldsymbol{a2} + \sqrt{\boldsymbol{a1} * \boldsymbol{a2}})$, where **a1** and **a2** are the areas of 2 serial sections and **i** is the interval (0.2-0.4 mm) between

them. Similar procedure was followed for the assessment of healthy muscular tissue volume.

Triphenyltetrazolium chloride staining. Murine hearts were cut in slices and stained in pre-warmed PBS supplemented with 1% TTC (2,3,5-Triphenyltetrazolium Chloride, Sigma), for 15 minutes at 37°C, then fixed in 4% PFA for 20 minutes. TTC technique represents a reliable, practical method to evaluate myocardial infarct size in the early phase after coronary occlusion. Damaged tissue was quantified in each section with ImageJ 1.52p software (National Institutes of Health) based on the staining. The percentage of damaged myocardial tissue volume was calculated as the sum of damaged volumes between serial sections normalized on the total myocardial tissue volume. The volume between serial sections was calculated with the formula of a truncated pyramid: $\frac{1}{3}\,\mathbf{i}\,(\boldsymbol{a1} + \boldsymbol{a2} + \sqrt{\boldsymbol{a1} * \boldsymbol{a2}})$, where **a1** and **a2** are the areas of 2 serial sections and **i** is the interval (2 mm) between them.

Screening of FDA-approved active GR agonists on cardiomyocyte cell cycle activity. Primary neonatal rat cardiomyocytes (CMs) were extracted from hearts of 0-day-old (P0) rats (Wistar strain). Hearts were harvested, washed in PBS and, after the removal of the atria, were placed into GentleMacs C tubes (# 130-093-237, Miltenyi). Cardiac tissue was dissociated using the gentleMACS Dissociator (#130-093-235, Miltenyi) in combination with the Neonatal Heart Dissociation Kit, mouse and rat (130-105-420 Miltenyi), according to manufacturer's instructions. A first depletion of non-CMs cells was performed by magnetic labelling using the Neonatal Cardiomyocyte Isolation Kit, rat (130-105-420, Miltenyi), in combination with the LD Column (130-042-901, Miltenyi), and the QuadroMACS Separator (130-090-976, Miltenyi), following manufacturer's instructions. The magnetically labelled non-target cells are retained within the column, thus allowing the unlabelled cardiomyocytes to run through. The collected primary rat neonatal cardiac myocytes were then resuspended in DMEM 4.5 g/l glucose (Life Technologies) supplemented with 5% FBS, 20 mg/ml vitamin B12 (Sigma), passed through a cell strainer (40 mm, BD Falcon) and then pre-plated in 10 cm dishes for 2h, in order to allow attachment of cardiac fibroblast only, thus performing a second depletion of non-CMs cells. Supernatant containing CMs was collected and CMs seeded in 384 well plate (PerkinElmer CellCarrierUltra-384 Black,

Optically Clear Bottom, Collagen Coated, Tissue Culture Treated) using a Multidrop™ Combi Reagent Dispenser (Thermo Fisher Scientific), in order to obtain homogeneous seeding of the cells. The next day, an intermediate dilution (50uM; 0.5% DMSO in DMEM) of the selected compounds (Prestwick Chemicals) was prepared using the Janus automated liquid handling station (PerkinElmer) and 10ul of this dilution was spotted on top of the cells, thus reaching a final concentration of 10uM with 0.1% DMSO. 28 hours after drug treatment, the cells were pulsed with 5- ethynyl-29-deoxyuridine (EdU, Thermo Fisher Scientific) at a final concentration of 10µM for 20 h. Cells were fixed in 4% PFA for 10 minutes, washed in Phosphate Buffer Saline (PBS) and processed for Immunofluorescence.

Cells were permeabilized with 0.5% Triton X-100 in PBS for 10 min, followed by 1 hour blocking in 1% BSA (Roche). Cardiomyocytes were then stained overnight at 4 °C with mouse monoclonal antibody against sarcomeric α-actinin (1:500, Abcam, ab9465) diluted in 1% BSA. Cells were washed with PBS and incubated for 2 hours with the secondary antibody conjugated to Alexa Fluor-488 (Thermo Fisher Scientific A-21202). Cells were further processed using the Click-IT EdU 594 Imaging kit (Thermo Fisher Scientific C10339) to reveal EdU incorporation, according to the manufacturer's instructions. Nuclei were stained with Hoechst 33342.

Image acquisition was performed using the Operetta CLS high content screening microscope (Perkin Elmer) with a Zeiss 20 x (NA=0.80) objective. A total of 9 fields per well were acquired and subsequently analysed, using the Harmony software (PerkinElmer), for cardiac α-Actinin expression (selection marker for cardiac myocytes) and EdU incorporation (DNA synthesis).

Data Availability

The datasets generated and/or analyzed in the current study are available in the source data file. RNA-seq data were deposited in the GEO repository under accession numbers GSE202968 and GSE202969.

Statistical analysis. Numerical data were collected using Excel (Microsoft 365) software and subsequent statistical analyses were performed with GraphPad 8.0.1 software (Prism). Whenever normality could be assumed the Student's t-test 2-sided or analysis of variance (ANOVA) followed by Tukey's or Sidak's test was used to

compare group means, as specified in the figure legends. P value<0.05 was considered to represent a statistically significant difference. In all panels, numerical data are presented as mean ± s.e.m. or median ± s.e.m, as specified in the figure legends.

ACKNOWLEDGMENTS

This project was supported by European Union's Horizon 2020 research and innovation programme under the ERA-NET on Cardio Vascular Diseases (ERA-CVD) Co-fund action to G.D'U. and E.T. (Grant Number: JCT2016-40-080), by Fondazione Luisa Fanti Melloni to G.D'U., by Fondazione Carisbo to G.D'U. (Grant number: 2020.0389), by Fondazione Cariplo to G.D'U. and M.L. (Grant Number: GR 2017-0800), by International Society for Heart Research to N.P. (ISHR research fellowship 2019), by University of Bologna AlmaIdea Junior grant INTACT to L.I., by University of Bologna AlmaIdea Junior grant to M.L. and by Ministry of Health - Ricerca Corrente - IRCCS MultiMedica. We thank Fondazione Dal Monte (Bologna, Italy) and Centro Studi della Barbariga (Noventa Padovana, Padua, Italy) for the financial support finalized to Anna Maria Porcelli for the acquisition of instruments Seahorse Xfe96 and Jasco V550 spectrophotometer, respectively. The funders had no role in study design, data collection and analysis, decision to publish or preparation of the manuscript.

We thank Prof. Giuseppe Pelosi, Dr. Donata Micello, Emanuela Paiola, Cristina Kluc, Alessandra Perlasca and Barnaba Rainoldi for technical assistance in sectioning of paraffin-embedded samples. Part of this work was carried out in ALEMBIC, an advanced microscopy laboratory established by IRCCS Ospedale San Raffaele and Università Vita-Salute San Raffaele. We thank Desiree Zambroni for the technical assistance in the *in vitro* immunofluorescence imaging.

AUTHOR CONTRIBUTIONS

N.P., F.S. and G.D'U. designed the experiments. N.P and F.S. carried out most of the experiments and analysed the data. K.-B.U, M.C. and G.D'U. performed myocardial infarction experiments and/or echocardiographic analyses. L.I. performed microrespirometry assays. S.D.P., C.B., C.M., F.P., E.P., R.S.P., M.M. performed immunofluorescence, western blots and gene expression analysis. V.P. performed TEM analyses. L.B. performed the screening of FDA-approved GR agonists. R.T. helped with immunofluorescence image acquisition and time-lapse imaging. G.D'U analysed

RNA-sequencing data. G.C., A.M.P., M.L., C.V., M.G., R.R. and E.T. supervised the experiments done by their laboratory members, and G.D'U supervised the entire project. N.P., F.S. and G.D'U wrote the manuscript with editing contributions from all of the authors.

COMPETING FINANCIAL INTERESTS

The authors declare no competing interests.

Figure legends

Figure 1. Exposure to physiological glucocorticoids (GCs) induces cell cycle exit and reduces the proliferation of neonatal cardiomyocytes via Glucocorticoid Receptor (GR) activation. (a-c) 1-day-old (P1) mouse cardiomyocytes (CMs) were cultured *in vitro* and stimulated with various doses of corticosterone (CORT); CMs were identified by cTnI or cTnT staining (see Methods for further details) and analysed by immunofluorescence for (**a**) cell cycle activity (Ki67, n = 24 samples with a total of 6333 CMs analysed), (**b**) DNA synthesis (BrdU, n = 42 samples with a total of 15462 CMs analysed) and (**c**) cytokinesis (Aurora B kinase, n = 21 samples with a total of 9761 CMs analysed); representative pictures are provided; arrows point at proliferating CMs; scale bars, 20 μm; (**d-e**) 16 hours time-lapse video quantification and representative images of (**d**) cell division and (**e**) binucleation events in CMs isolated from P1 mice, labelled with TMRE (see Methods for details), cultured *in vitro* and treated with CORT (n = 12 samples with a total of 5814 CMs); arrows point at CMs undergoing cell cycle events; time of acquisition (hours:minutes:seconds) is indicated; scale bar, 10 μm; (**f-g**) *In vitro* evaluation of cardiomyocyte (CM) (**f**) cell cycle activity by Ki67 (n = 42 samples with a total of 7693 CMs) and (**g**) DNA synthesis by BrdU incorporation assay (n = 67 samples with a total of 27315 CMs) upon treatment with CORT and small inhibitory molecules for GR (RU486) or MR (Eplerenone); **(h)** Neonatal rat cardiomyocytes were cultured *in vitro*, stimulated with FDA approved GR agonists and analysed for DNA synthesis (EdU) (n = 32). In all panels, numerical data are presented as mean (error bars show s.e.m.); statistical significance was determined using one-way ANOVA followed by Tukey's test in **a, b, c, f, g, h** and 2-sided Student's t-test in **d**.

Figure 2. A transient increase in Glucocorticoid Receptor (GR) abundance concurs to cardiomyocyte withdrawal during the early postnatal period. (a) mRNA expression levels of Glucocorticoid Receptor (GR) in postnatal day 1 (P1), postnatal day 3 (P3), postnatal day 5 (P5), postnatal day 7 (P7), postnatal day 14 (P14), postnatal day 28 (P28) and postnatal day 56 (P56) heart lysates (n = 43 mice); (**b**) Western blot analysis of GR in P1 and P7 heart lysates (n = 6 mice); representative pictures and quantifications are provided; (**c**) GR mRNA expression levels in cardiomyocytes and stromal cells isolated from postnatal day 1 (P1) and postnatal day 7 (P7) hearts (n = 12 mice); (**d**) Immunofluorescence analysis of GR in P1 and P7 left ventricular heart sections (n = 6 mice with a total of 2592 analysed CMs), showing similar nuclear localization of GR in cardiomyocytes; scalebars, 15 μm; (**e**) *In vivo* evaluation of cardiomyocyte (CM) cell cycle activity by Ki67 and cTnT staining in heart sections from P7 mice with/without administration of RU486 in the drinking water starting from birth (n = 6 mice with a total of 9496 CMs analysed); representative images are provided, arrows point at proliferating CMs; scale bars, 25 μm. In all panels, numerical data are presented as mean (error bars show s.e.m.); statistical significance was determined using 2-sided Student's t-test.

Figure 3. *In vitro* proliferation of neonatal cardiomyocytes is increased by cardiomyocyte-specific deletion of the Glucocorticoid Receptor (GR-cKO). (a) A schematic diagram depicting the generation of cardiomyocyte-restricted GR knock-out (GR-cKO) mice; (**b**) Western Blot analysis of GR protein levels in neonatal (P1) control (ctrl) and GR-cKO heart lysates (hearts isolated in a single session from n = 4 littermates mice); (**c-e**) Immunofluorescence analysis of (**c**) cell cycle activity (Ki67, n = 6 samples with a total of 2335 CMs analysed), (**d**) DNA synthesis (BrdU, n = 15 samples with a total of 4027 CMs analysed) and (**e**) cytokinesis (Aurora B kinase, n = 6 samples with a total of 3655 CMs analysed) in cardiomyocytes isolated from P1 ctrl and GR-cKO mice; representative pictures are provided; arrows point at proliferating cardiomyocytes; scale bars, 25 μm; (**f-g**) 16 hours time-lapse video quantification and representative images of (**f**) cell division and (**g**) binucleation events in CMs isolated from P1 ctrl and GR-cKO mice, labelled with TMRE (see Methods for details) and cultured *in vitro* (n = 11 samples with a total of 5527 CMs); arrows point at CMs undergoing cell cycle events; time of acquisition (h:m:s) is indicated; scale bar, 10 μm.

In all panels, numerical data are presented as mean (error bars show s.e.m.); statistical significance was determined using 2-sided Student's t-test.

Figure 4. GR-cKO reduces the hyperplastic to hypertrophic transition occurring during the early postnatal cardiac development. (a) Heart weight / body weight (HW/BW) ratio in P7 control and GR-cKO mice (n = 94 mice); (**b**) Cardiomyocyte (CM) cross-sectional area evaluation by immunofluorescence analysis of wheat germ agglutinin (WGA) on P7 control and GR-cKO ventricular heart sections (n = 600 CMs pooled from the analysis of 6 murine hearts isolated in two independent experiments), representative images are provided; scale bars, 25 μm; (**c**) Stereological estimation of cardiomyocyte number in P7 ctrl and GR-cKO hearts (see Material and methods for details, n = 6 mice); (**d-e**) *In vivo* evaluation of CM proliferation in control and GR-cKO ventricular heart sections; CMs were identified by cTnI or cTnT staining (see Methods for further details), proliferation was evaluated by immunofluorescence analysis of (**d**) Ki67 (n = 6 mice with a total of 20859 CMs analysed) and (**e**) mid-body Aurora B kinase (n = 7 mice with a total of 7988 CMs analysed); representative images are provided, arrows point at proliferating CMs; scale bars 10 μm; **(f)** Fraction of mono-nucleated and bi-nucleated cardiomyocytes in P7 control and GR-cKO cardiomyocytes cultured *in vitro* (n = 6 samples with a total of 1275 CMs analysed); (**g**) Schematic diagram showing the role of GR in promoting the postnatal developmental transition of neonatal cardiomyocyte from hyperplastic to hypertrophic growth during the early postnatal development. In all panels, numerical data are presented as mean in **a, c, d, e, f** and median in **b** (error bars show s.e.m.); statistical significance was determined using 2-sided Student's t-test.

Figure 5. GR promotes the maturation of myofibrils-mitochondria organization and metabolic rewiring occurring during the early postnatal development. (**a-f**) Ultrastructure analysis by transmission electron microscopy (TEM) of (**a-c**) P7 control and (**d-f**) GR-cKO heart sections (n = 6 murine hearts isolated in two independent experiments): control P7 cardiomyocytes show organized myofibrillar architecture (dotted lines in **a,** magnification of sarcomere in **c**) in close contact with clusters of mitochondria (arrows in **a,** magnification in **b**), whereas GR-cKO cardiomyocytes show irregular and immature myofibrils (dotted lines in **d,** magnification in **f**) arranged around isolated not organized mitochondria (yellow arrows in **d,** magnification in **e**);

GR-cKO cardiomyocytes also show lipid droplets (white arrows in **d)**; scale bars 2 μm, 500 nm for magnifications; (**g**) Schematic diagram showing the role of GR in promoting maturation of sarcomere-mitochondrial organization in cardiomyocytes during the early postnatal development. Legend for electron microscopy images: N = nucleus; S = sarcomere unit; H = H band; A = A band; I = I band; M = M band; Z = Z line.

Figure 6. Ablation of GR promotes cardiomyocyte proliferation by favouring glucose catabolism over fatty acid oxidation. (a) Gene ontology analysis according to Biological Process of RNA-Seq data of cultured P1 GR-cKO versus control cardiac cell cultures (n = 6 mice); (**b**) Heatmaps of statistically significant differentially expressed genes (pvalue < 0.05) by RNA-Seq transcriptome analysis of P1 GR-cKO versus control cardiac cell cultures (n = 6 mice) according to the following gene ontology terms (Gene Ontology: Biological Process): glycolytic process (GO: 0006096); **(c)** Gene ontology analysis according to Biological Process of RNA-Seq data of P7 GR-cKO versus control hearts (n = 6 mice); (**d-f**) Heatmaps of statistically significant differentially expressed genes (pvalue < 0.05) by RNA-Seq transcriptome analysis of P7 GR-cKO versus controls hearts (n = 6 mice) according to the following gene ontology terms (Gene Ontology: Biological Process): NADP metabolic process (GO:0006739 in **d**), fatty acid oxidation (GO:0019395 in **e**) and mitochondrial ATP synthesis coupled electron transport (GO:0042775 in **f**); (**g**) Analysis of oxygen consumption rate (OCR) by Seahorse microrespirometer in GR-cKO versus control P1 cardiomyocyte cultured *in vitro* (n = 7 samples)*;* (**h**) Quantification of spare respiratory capacity in GR-cKO versus control P1 cardiomyocytes cultured *in vitro* (n = 7 samples); (**i**) Quantification of the contribution of fatty acid oxidation (FAO) to OCR after inhibition of FAO with etomoxir in GR-cKO versus control P1 cardiomyocytes cultured *in vitro* (n = 8 samples); (**j**) Immunofluorescence analysis of DNA synthesis (BrdU, n = 12 samples with a total of 3325 CMs analysed) in cardiomyocytes isolated from P1 ctrl and GR-cKO mice treated with 2-deoxy-glucose (2dG, 3mM). In all panels, numerical data are presented as mean (error bars show s.e.m.); statistical significance was determined using 2-sided Student's t-test in **h, i** and one-way ANOVA followed by Sidak's test in **j**.

Figure 7. GR ablation enhances mammalian cardiac regenerative ability. (a) Experimental design for the analysis of cardiomyocyte (CM) dedifferentiation and

proliferation after myocardial infarction (MI) in control/GR-cKO mice at juvenile (postnatal day 7 - P7) stage ; (**b-c**) *in vivo* evaluation of CM cell cycle re-entry (Ki67+, **b**) and sarcomere marginalization (**c**) by Ki67/TroponinT immunofluorescence analysis in control/GR-cKO heart sections 10 days post-MI (n = 8 mice with a total of 36555 CMs analysed); representative pictures of cell cycle activity with/without sarcomere structure marginalization in GR-cKO border zone are provided; arrows point at proliferating cardiomyocytes; scale bars, 25 µm; (**d**) *in vivo* evaluation of AuroraB+ CMs (n = 8 mice with a total of 15161 CMs analysed); representative pictures are provided; scale bars, 20 µm; (**e**) *in vivo* evaluation of CM cell cycle re-entry by Ki67/ TroponinT immunofluorescence analysis of heart sections of control/GR-cKO adult uninjured mice (~8 weeks-old, n = 6 mice with a total of 8504 CMs analysed); **(f)** Experimental design for cardiac regeneration analysis following injury in adult (10-12 weeks-old) control/GR-cKO mice; (**g**) *in vivo* evaluation of cardioprotection by triphenyltetrazolium chloride staining in control/GR-cKO heart sections 1 day post-MI (n=13 mice); representative pictures are provided; scale bar, 1 mm; (**h-i**) *in vivo* evaluation of adult CM cell cycle re-entry by Ki67 immunofluorescence analysis in control/GR-cKO heart sections (**h**) 11 days post-MI (n= 11 mice with a total of 24514 CMs analysed) and (**i**) ~1 month post-MI (n = 6 mice with a total of 26349 CMs analysed)**;** representative pictures of cell cycle activity in GR-cKO border zone are provided; scale bars 25 µm; **(j)** Scar volume and healthy tissue volume analysis based on Masson's trichrome staining of serial heart sections of control/GR-cKO mice ~1 month post-MI (n = 8 mice); representative pictures are provided; scale bar, 1 mm; (**k**) Serial echocardiographic measurements of ejection fraction (EF) of injured control/GR-cKO adult mice (n = 11 mice); representative images of M-mode echocardiographic analyses are provided; scale bars, 2 mm (vertical axis) and 200 ms (horizontal axis). In all panels numerical data are presented as mean (error bars show s.e.m.); statistical significance was determined using 2-sided Student's t-test.

Figure 8. Pharmacological inhibition of GR enhances regenerative potential of the adult mouse heart after myocardial infarction. (a) Cardiomyocytes isolated from P1 mice were treated with corticosterone for 24 hours and then, immediately or after 24 or 48 hours of recovery with normal medium, assessed for DNA synthesis (BrdU, n = 14 samples with a total of 3833 CMs analysed) by immunofluorescence analysis; **(b)**

Experimental design for analysis of the effects of the transient GR blockage following myocardial injury in adult mice; (**c-d**) *in vivo* evaluation of cardiomyocyte (CM) cell cycle re-entry by immunofluorescence analysis of Ki67 and cardiac Troponin T in heart sections of normal feed (control) and RU486 treated animals (**c**) 14 days post-MI (n = 7 mice with a total of 24656 CMs analysed) and (**d**) 35 days post-MI (21 days after the end of RU486 treatment) (n = 8 mice with a total of 20031 CMs analysed), according to the scheme in **b**; representative pictures of cell cycle activity in the border zone of RU486 treated hearts are provided; arrows point at proliferating cardiomyocytes; scale bar, 25 µm; (**e**) *in vivo* evaluation of Aurora B kinase positive CMs 14 days following MI (n = 7 mice with a total of 19160 CMs analysed); **(f)** Scar and healthy tissue volume analysis based on Masson's trichrome staining of serial heart sections of control and RU486 treated mice, 35 days post-MI (n = 14 mice); representative pictures are provided; scale bars, 1 mm; (**g**) Serial echocardiographic measurements of ejection fraction (EF) of injured control and injured RU486 treated adult mice (n = 18 mice), according to the scheme in **b**; representative images of M-mode echocardiographic analyses are provided. In all panels numerical data are presented as mean (error bars show s.e.m.); statistical significance was determined using one-way ANOVA followed by Sidak's test in **a**, and 2-sided Student's t-test in **c,e**, **f, g**).

REFERENCES

1. Bongiovanni, C. *et al.* Reawakening the Intrinsic Cardiac Regenerative Potential: Molecular Strategies to Boost Dedifferentiation and Proliferation of Endogenous Cardiomyocytes. *Front. Cardiovasc. Med.* **8**, 750604 (2021).
2. Tzahor, E. & Poss, K. D. Cardiac regeneration strategies: Staying young at heart. *Science* **356**, 1035–1039 (2017).
3. Sadek, H. & Olson, E. N. Toward the Goal of Human Heart Regeneration. *Cell Stem Cell* **26**, 7–16 (2020).
4. Eschenhagen, T. *et al.* Cardiomyocyte Regeneration: A Consensus Statement. *Circulation* **136**, 680–686 (2017).
5. van Berlo, J. H. & Molkentin, J. D. An emerging consensus on cardiac regeneration. *Nat. Med.* **20**, 1386–93 (2014).
6. Porrello, E. R. *et al.* Transient regenerative potential of the neonatal mouse heart. *Science* **331**, 1078–80 (2011).
7. Drenckhahn, J.-D. *et al.* Compensatory growth of healthy cardiac cells in the presence of diseased cells restores tissue homeostasis during heart development. *Dev. Cell* **15**, 521–33 (2008).
8. Sampaio-Pinto, V. *et al.* Neonatal Apex Resection Triggers Cardiomyocyte

Proliferation, Neovascularization and Functional Recovery Despite Local Fibrosis. *Stem cell reports* **10**, 860–874 (2018).

9. Haubner, B. J. *et al.* Complete cardiac regeneration in a mouse model of myocardial infarction. *Aging (Albany. NY).* **4**, 966–77 (2012).

10. Ye, L. *et al.* Early Regenerative Capacity in the Porcine Heart. *Circulation* **138**, 2798–2808 (2018).

11. Zhu, W. *et al.* Regenerative Potential of Neonatal Porcine Hearts. *Circulation* **138**, 2809–2816 (2018).

12. Li, Y. *et al.* Genetic Tracing Identifies Early Segregation of the Cardiomyocyte and Nonmyocyte Lineages. *Circ. Res.* **125**, 343–355 (2019).

13. Jopling, C. *et al.* Zebrafish heart regeneration occurs by cardiomyocyte dedifferentiation and proliferation. *Nature* **464**, 606–9 (2010).

14. Kikuchi, K. *et al.* Primary contribution to zebrafish heart regeneration by gata4(+) cardiomyocytes. *Nature* **464**, 601–5 (2010).

15. Soonpaa, M. H., Kim, K. K., Pajak, L., Franklin, M. & Field, L. J. Cardiomyocyte DNA synthesis and binucleation during murine development. *Am. J. Physiol.* **271**, H2183-9 (1996).

16. Li, F., Wang, X., Capasso, J. M. & Gerdes, A. M. Rapid transition of cardiac myocytes from hyperplasia to hypertrophy during postnatal development. *J. Mol. Cell. Cardiol.* **28**, 1737–46 (1996).

17. Bergmann, O. *et al.* Evidence for cardiomyocyte renewal in humans. *Science* **324**, 98–102 (2009).

18. Senyo, S. E. *et al.* Mammalian heart renewal by pre-existing cardiomyocytes. *Nature* **493**, 433–436 (2013).

19. Uygur, A. & Lee, R. T. Mechanisms of Cardiac Regeneration. *Dev. Cell* **36**, 362–74 (2016).

20. Heallen, T. R., Kadow, Z. A., Kim, J. H., Wang, J. & Martin, J. F. Stimulating Cardiogenesis as a Treatment for Heart Failure. *Circ. Res.* **124**, 1647–1657 (2019).

21. Hashimoto, H., Olson, E. N. & Bassel-Duby, R. Therapeutic approaches for cardiac regeneration and repair. *Nat. Rev. Cardiol.* **15**, 585–600 (2018).

22. Cahill, T. J., Choudhury, R. P. & Riley, P. R. Heart regeneration and repair after myocardial infarction: translational opportunities for novel therapeutics. *Nat. Rev. Drug Discov.* **16**, 699–717 (2017).

23. Galdos, F. X. *et al.* Cardiac Regeneration: Lessons From Development. *Circ. Res.* **120**, 941–959 (2017).

24. Oakley, R. H. & Cidlowski, J. A. Glucocorticoid signaling in the heart: A cardiomyocyte perspective. *J. Steroid Biochem. Mol. Biol.* **153**, 27–34 (2015).

25. Richardson, R. V., Batchen, E. J., Denvir, M. A., Gray, G. A. & Chapman, K. E. Cardiac GR and MR: From Development to Pathology. *Trends Endocrinol. Metab.* **27**, 35–43 (2016).

26. Rog-Zielinska, E. A., Richardson, R. V., Denvir, M. A. & Chapman, K. E.

Glucocorticoids and foetal heart maturation; implications for prematurity and foetal programming. *J. Mol. Endocrinol.* **52**, R125-35 (2014).

27. Giraud, G. D., Louey, S., Jonker, S., Schultz, J. & Thornburg, K. L. Cortisol stimulates cell cycle activity in the cardiomyocyte of the sheep fetus. *Endocrinology* **147**, 3643–9 (2006).

28. Feng, X., Reini, S. A., Richards, E., Wood, C. E. & Keller-Wood, M. Cortisol stimulates proliferation and apoptosis in the late gestation fetal heart: differential effects of mineralocorticoid and glucocorticoid receptors. *Am. J. Physiol. Regul. Integr. Comp. Physiol.* **305**, R343-50 (2013).

29. de Vries, W. B. *et al.* Suppression of physiological cardiomyocyte proliferation in the rat pup after neonatal glucocorticosteroid treatment. *Basic Res. Cardiol.* **101**, 36–42 (2006).

30. Gay, M. S., Li, Y., Xiong, F., Lin, T. & Zhang, L. Dexamethasone treatment of newborn rats decreases cardiomyocyte endowment in the developing heart through epigenetic modifications. *PLoS One* **10**, e0125033 (2015).

31. Cutie, S., Payumo, A. Y., Lunn, D. & Huang, G. N. In vitro and in vivo roles of glucocorticoid and vitamin D receptors in the control of neonatal cardiomyocyte proliferative potential. *J. Mol. Cell. Cardiol.* **142**, 126–134 (2020).

32. Tao, Z. *et al.* Dexamethasone inhibits regeneration and causes ventricular aneurysm in the neonatal porcine heart after myocardial infarction. *J. Mol. Cell. Cardiol.* **144**, 15–23 (2020).

33. Hattori, F. *et al.* Nongenetic method for purifying stem cell-derived cardiomyocytes. *Nat. Methods* **7**, 61–6 (2010).

34. Genangeli, M. *et al.* Development and application of a UHPLC-MS/MS method for the simultaneous determination of 17 steroidal hormones in equine serum. *J. Mass Spectrom.* **52**, 22–29 (2017).

35. Morgan, R. A. *et al.* Dysregulation of cortisol metabolism in equine pituitary pars intermedia dysfunction. *Endocrinology* **159**, 3791–3800 (2018).

36. Perogamvros, I., Ray, D. W. & Trainer, P. J. Regulation of cortisol bioavailability--effects on hormone measurement and action. *Nat. Rev. Endocrinol.* **8**, 717–27 (2012).

37. Savu, L., Nunez, E. & Jayle, M. F. Corticosterone binding by mouse sera during foetal and post-natal development. *Acta Endocrinol. (Copenh).* **84**, 177–90 (1977).

38. Oakley, R. H. *et al.* Essential role of stress hormone signaling in cardiomyocytes for the prevention of heart disease. *Proc. Natl. Acad. Sci. U. S. A.* **110**, 17035–40 (2013).

39. Ali, H., Braga, L. & Giacca, M. Cardiac regeneration and remodelling of the cardiomyocyte cytoarchitecture. *FEBS J.* **287**, 417–438 (2020).

40. Piquereau, J. & Ventura-Clapier, R. Maturation of Cardiac Energy Metabolism During Perinatal Development. *Front. Physiol.* **9**, 959 (2018).

41. Bae, J., Paltzer, W. G. & Mahmoud, A. I. The Role of Metabolism in Heart Failure and Regeneration. *Front. Cardiovasc. Med.* **8**, 702920 (2021).

42. Sim, C. B. *et al.* Sex-Specific Control of Human Heart Maturation by the Progesterone Receptor. *Circulation* **143**, 1614–1628 (2021).

43. Kubin, T. *et al.* Oncostatin M is a major mediator of cardiomyocyte dedifferentiation and remodeling. *Cell Stem Cell* **9**, 420–32 (2011).

44. D'Uva, G. *et al.* ERBB2 triggers mammalian heart regeneration by promoting cardiomyocyte dedifferentiation and proliferation. *Nat. Cell Biol.* **17**, 627–38 (2015).

45. Puente, B. N. *et al.* The oxygen-rich postnatal environment induces cardiomyocyte cell-cycle arrest through DNA damage response. *Cell* **157**, 565–79 (2014).

46. Honkoop, H. *et al.* Single-cell analysis uncovers that metabolic reprogramming by ErbB2 signaling is essential for cardiomyocyte proliferation in the regenerating heart. *Elife* **8**, 1–65 (2019).

47. Cardoso, A. C. *et al.* Mitochondrial substrate utilization regulates cardiomyocyte cell-cycle progression. *Nat. Metab.* **2**, 167–178 (2020).

48. Mills, R. J. *et al.* Functional screening in human cardiac organoids reveals a metabolic mechanism for cardiomyocyte cell cycle arrest. *Proc. Natl. Acad. Sci. U. S. A.* **114**, E8372–E8381 (2017).

49. Cao, T. *et al.* Fatty Acid Oxidation Promotes Cardiomyocyte Proliferation Rate but Does Not Change Cardiomyocyte Number in Infant Mice. *Front. cell Dev. Biol.* **7**, 42 (2019).

50. Severinova, E. *et al.* Glucocorticoid Receptor-Binding and Transcriptome Signature in Cardiomyocytes. *J. Am. Heart Assoc.* **8**, (2019).

51. Talman, V. *et al.* Molecular Atlas of Postnatal Mouse Heart Development. *J. Am. Heart Assoc.* **7**, e010378 (2018).

52. Parikh, S. S. *et al.* Thyroid and Glucocorticoid Hormones Promote Functional T-Tubule Development in Human-Induced Pluripotent Stem Cell-Derived Cardiomyocytes. *Circ. Res.* **121**, 1323–1330 (2017).

53. Karbassi, E. *et al.* Cardiomyocyte maturation: advances in knowledge and implications for regenerative medicine. *Nat. Rev. Cardiol.* **17**, 341–359 (2020).

54. Hirose, K. *et al.* Evidence for hormonal control of heart regenerative capacity during endothermy acquisition. *Science (80-.).* **364**, 184–188 (2019).

55. Su, Q.-Q., Huang, X.-L., Qin, J. & Liu, Q.-S. Assessment of effects of mifepristone administration to lactating mice on the development and fertility of their progeny. *J. Obstet. Gynaecol. Res.* **41**, 575–81 (2015).

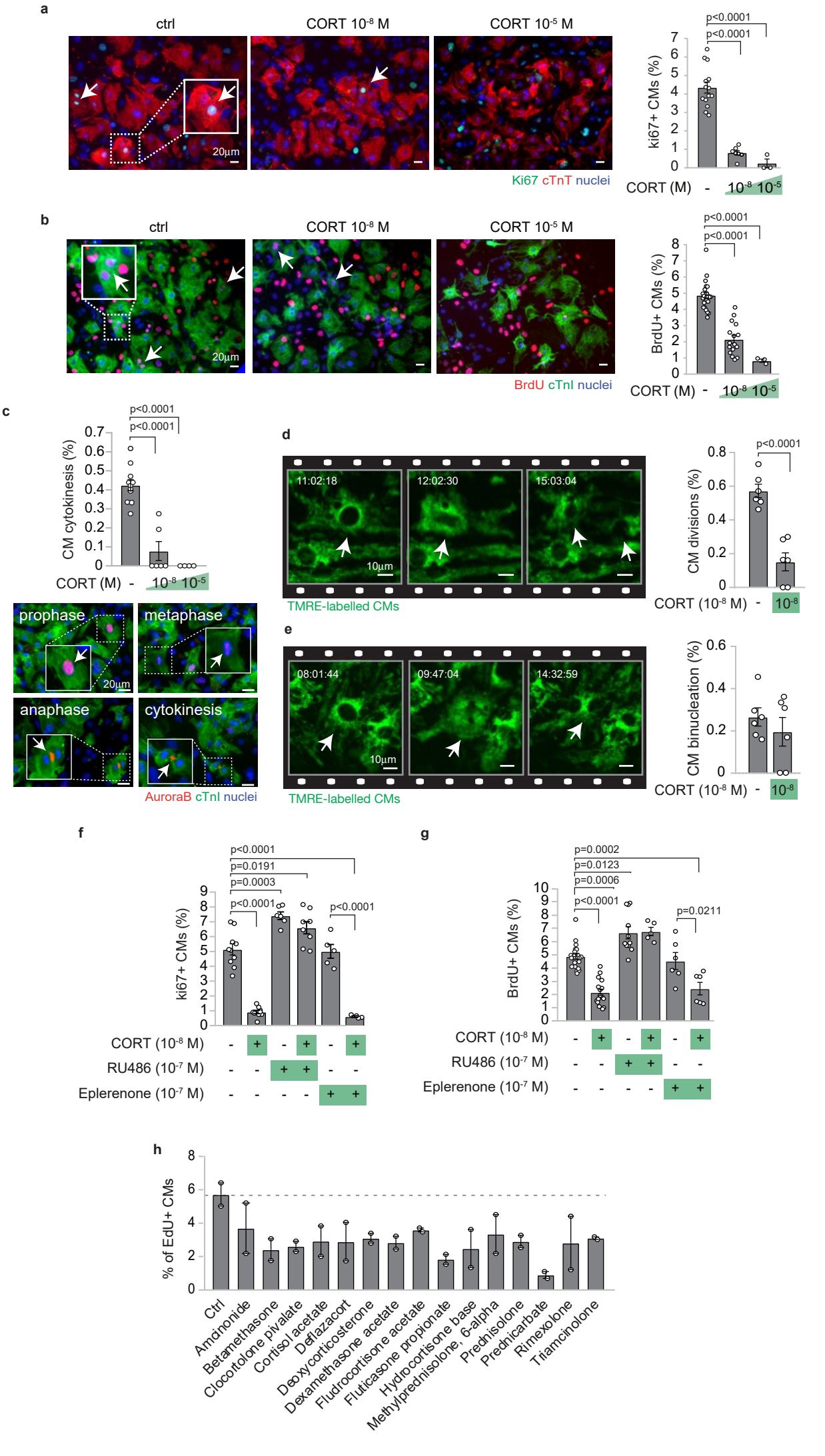
a
ctrl
CORT 10-8 M
CORT 10-5 M
20µm
Ki67 cTnT nuclei
ki67+ CMs (%)
p<0.0001
p<0.0001
CORT (M) - 10-8 10-5
b
ctrl
CORT 10-8 M
CORT 10-5 M
20µm
BrdU cTnI nuclei
BrdU+ CMs (%)
p<0.0001
p<0.0001
CORT (M) - 10-8 10-5
c
CM cytokinesis (%)
p<0.0001
p<0.0001
CORT (M) - 10-8 10-5
prophase
metaphase
anaphase
cytokinesis
20µm
AuroraB cTnI nuclei
d
11:02:18
12:02:30
15:03:04
10µm
TMRE-labelled CMs
CM divisions (%)
p<0.0001
CORT (10-8 M) - 10-8
e
08:01:44
09:47:04
14:32:59
10µm
TMRE-labelled CMs
CM binucleation (%)
CORT (10-8 M) - 10-8
f
ki67+ CMs (%)
p<0.0001
p=0.0191
p=0.0003
p<0.0001
p<0.0001
CORT (10-8 M) - + - + - +
RU486 (10-7 M) - - + + - -
Eplerenone (10-7 M) - - - - + +
g
BrdU+ CMs (%)
p=0.0002
p=0.0123
p=0.0006
p<0.0001
p=0.0211
CORT (10-8 M) - + - + - +
RU486 (10-7 M) - - + + - -
Eplerenone (10-7 M) - - - - + +
h
% of EdU+ CMs
Ctrl
Amcinonide
Betamethasone
Clocortolone pivalate
Cortisol acetate
Deflazacort
Deoxycorticosterone
Dexamethasone acetate
Fludrocortisone acetate
Fluticasone propionate
Hydrocortisone base
Methylprednisolone, 6-alpha
Prednisolone
Prednicarbate
Rimexolone
Triamcinolone

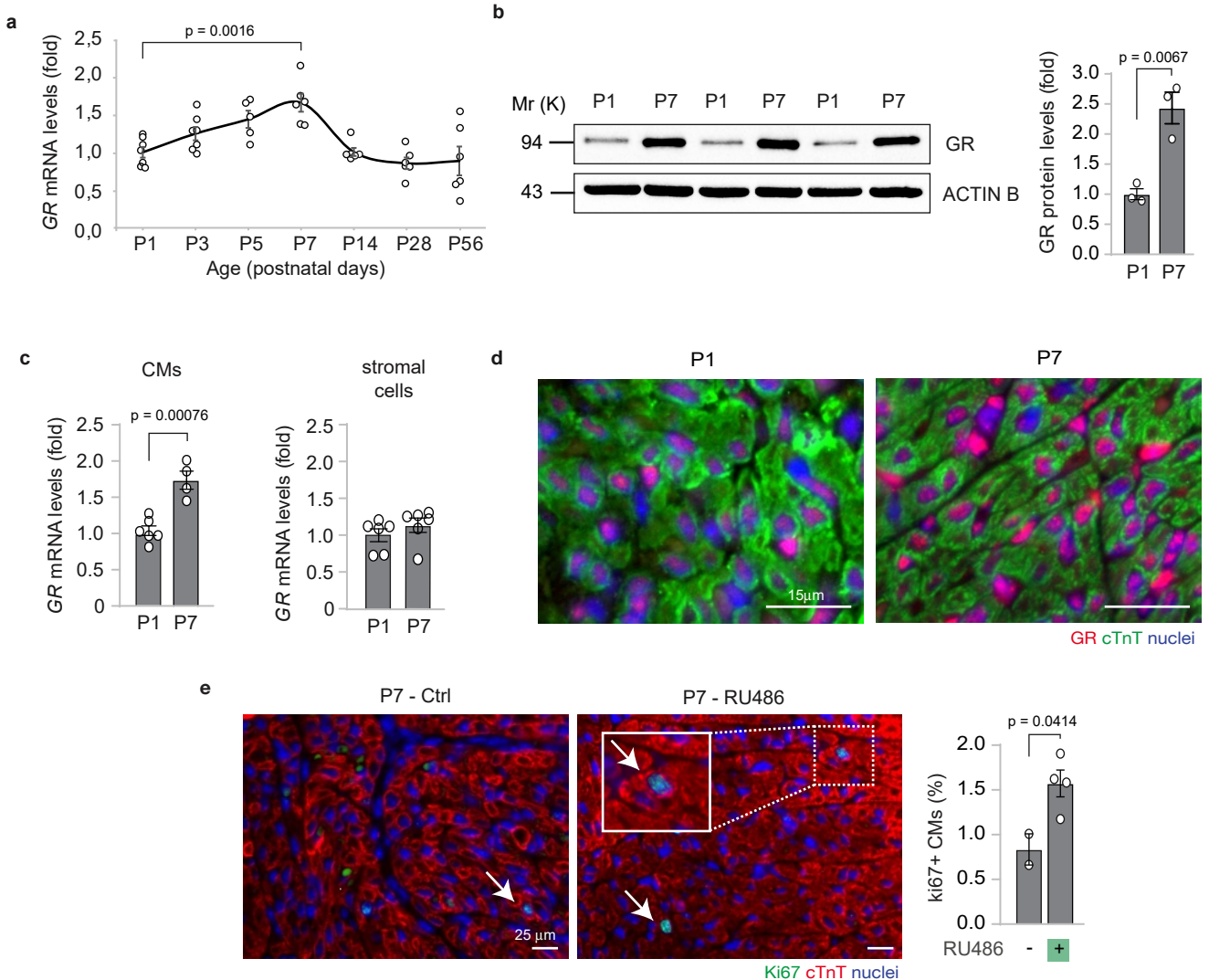
a
p = 0.0016
GR mRNA levels (fold)
2,5
2,0
1,5
1,0
0,5
0,0
P1
P3
P5
P7
P14
P28
P56
Age (postnatal days)
b
Mr (K)
P1
P7
P1
P7
P1
P7
94
GR
43
ACTIN B
p = 0.0067
GR protein levels (fold)
3.0
2.5
2.0
1.5
1.0
0.5
0.0
P1
P7
c
CMs
p = 0.00076
GR mRNA levels (fold)
2.5
2.0
1.5
1.0
0.5
0
P1
P7
stromal cells
GR mRNA levels (fold)
2.5
2.0
1.5
1.0
0.5
0
P1
P7
d
P1
P7
15µm
GR cTnT nuclei
e
P7 - Ctrl
P7 - RU486
25 µm
Ki67 cTnT nuclei
p = 0.0414
ki67+ CMs (%)
2.0
1.5
1.0
0.5
0.0
RU486
-
+

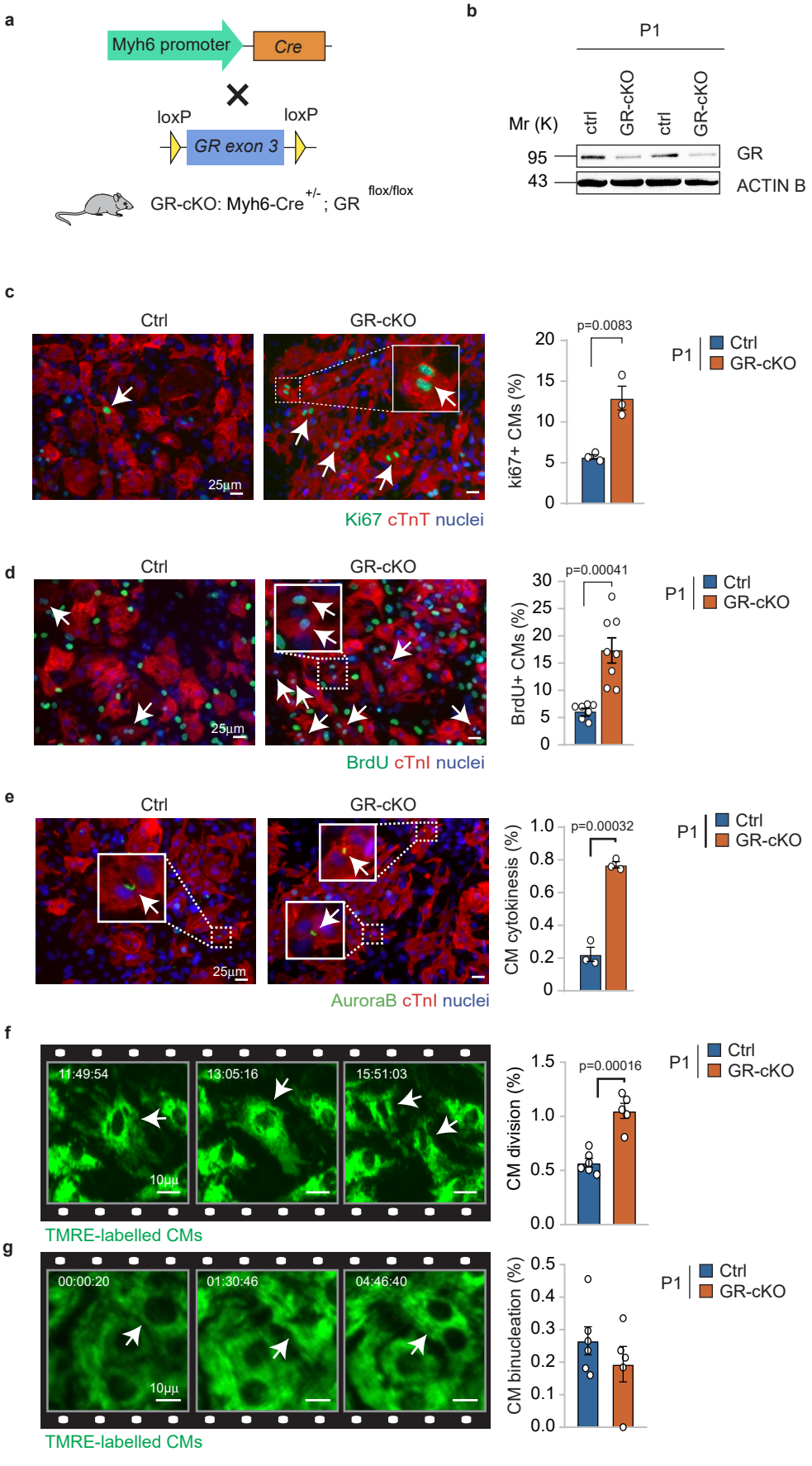
a
Myh6 promoter
Cre
loxP
loxP
GR exon 3
GR-cKO: Myh6-Cre+/- ; GR flox/flox
b
P1
Mr (K)
ctrl
GR-cKO
ctrl
GR-cKO
95
43
GR
ACTIN B
c
Ctrl
GR-cKO
25µm
Ki67 cTnT nuclei
p=0.0083
ki67+ CMs (%)
P1
Ctrl
GR-cKO
d
Ctrl
GR-cKO
25µm
BrdU cTnI nuclei
p=0.00041
BrdU+ CMs (%)
P1
Ctrl
GR-cKO
e
Ctrl
GR-cKO
25µm
AuroraB cTnI nuclei
p=0.00032
CM cytokinesis (%)
P1
Ctrl
GR-cKO
f
11:49:54
13:05:16
15:51:03
10µm
TMRE-labelled CMs
p=0.00016
CM division (%)
P1
Ctrl
GR-cKO
g
00:00:20
01:30:46
04:46:40
10µm
TMRE-labelled CMs
CM binucleation (%)
P1
Ctrl
GR-cKO

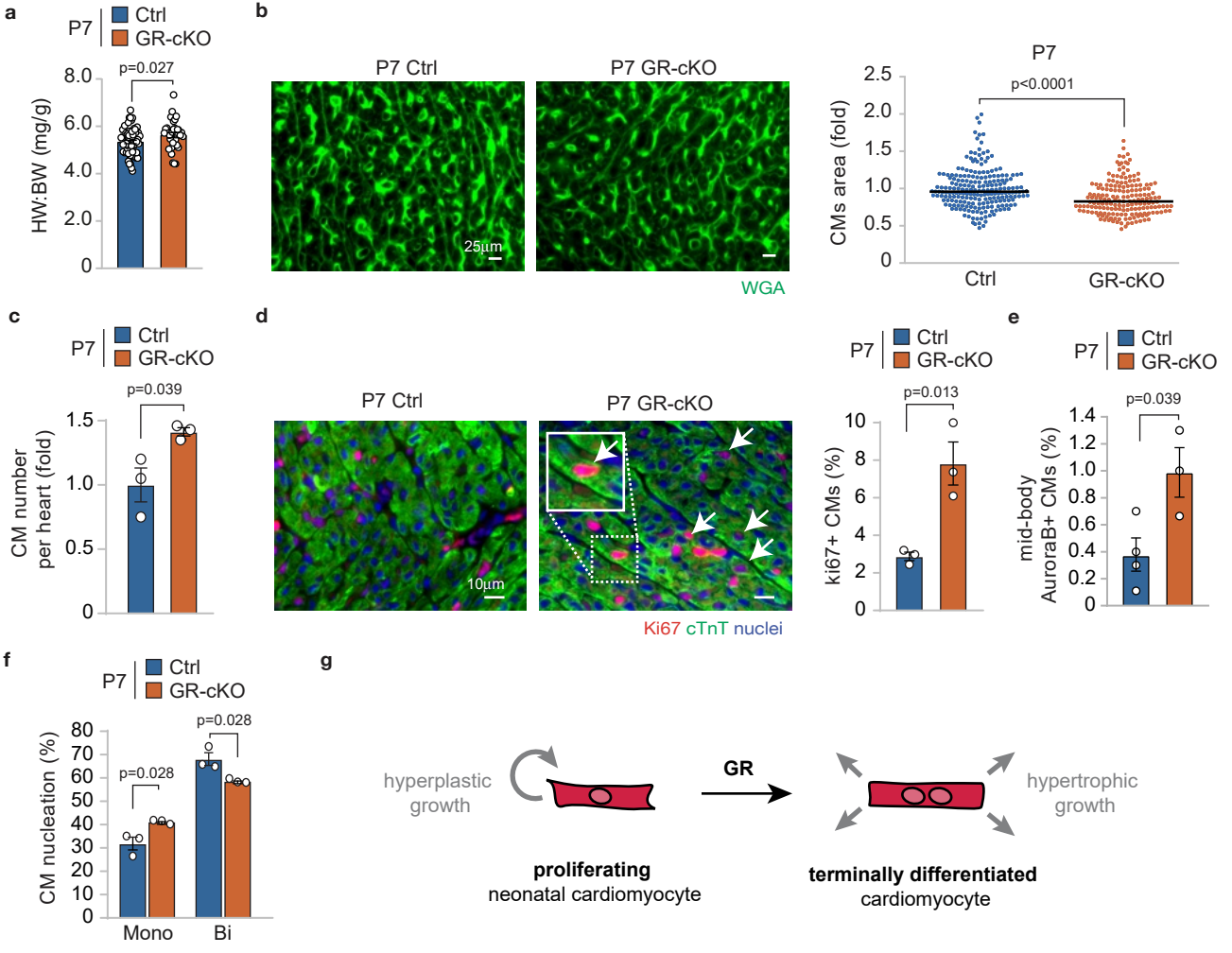
a
P7
Ctrl
GR-cKO
p=0.027
HW:BW (mg/g)
8.0
6.0
4.0
2.0
0
b
P7 Ctrl
P7 GR-cKO
25µm
WGA
P7
p<0.0001
CMs area (fold)
2.5
2.0
1.5
1.0
0.5
0
Ctrl
GR-cKO
c
P7
Ctrl
GR-cKO
p=0.039
CM number per heart (fold)
1.5
1.0
0.5
0
d
P7 Ctrl
P7 GR-cKO
10µm
Ki67 cTnT nuclei
P7
Ctrl
GR-cKO
p=0.013
ki67+ CMs (%)
10
8
6
4
2
0
e
P7
Ctrl
GR-cKO
p=0.039
mid-body AuroraB+ CMs (%)
1.4
1.2
1.0
0.8
0.6
0.4
0.2
0
f
P7
Ctrl
GR-cKO
p=0.028
p=0.028
CM nucleation (%)
80
70
60
50
40
30
20
10
0
Mono
Bi
g
hyperplastic growth
GR
hypertrophic growth
proliferating
neonatal cardiomyocyte
terminally differentiated
cardiomyocyte

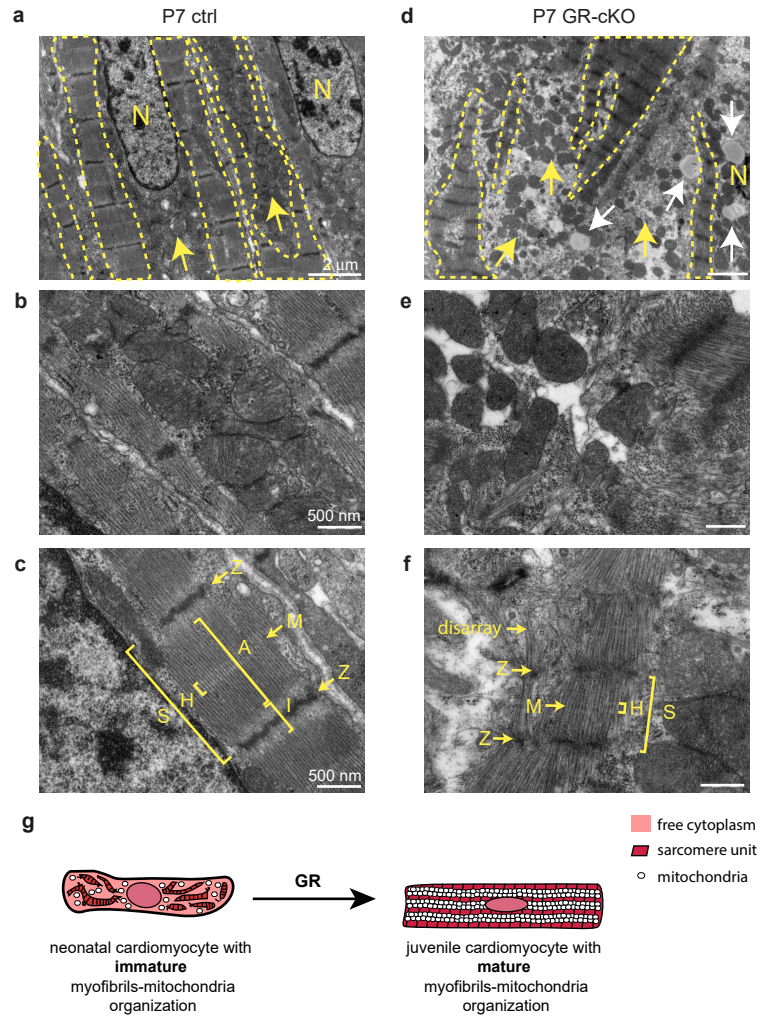
a
P7 ctrl
N
N
2 µm
d
P7 GR-cKO
N
b
500 nm
e
c
Z
M
A
Z
H
I
S
500 nm
f
disarray
Z
M
H
S
Z
g
free cytoplasm
sarcomere unit
mitochondria
GR
neonatal cardiomyocyte with
immature
myofibrils-mitochondria
organization
juvenile cardiomyocyte with
mature
myofibrils-mitochondria
organization

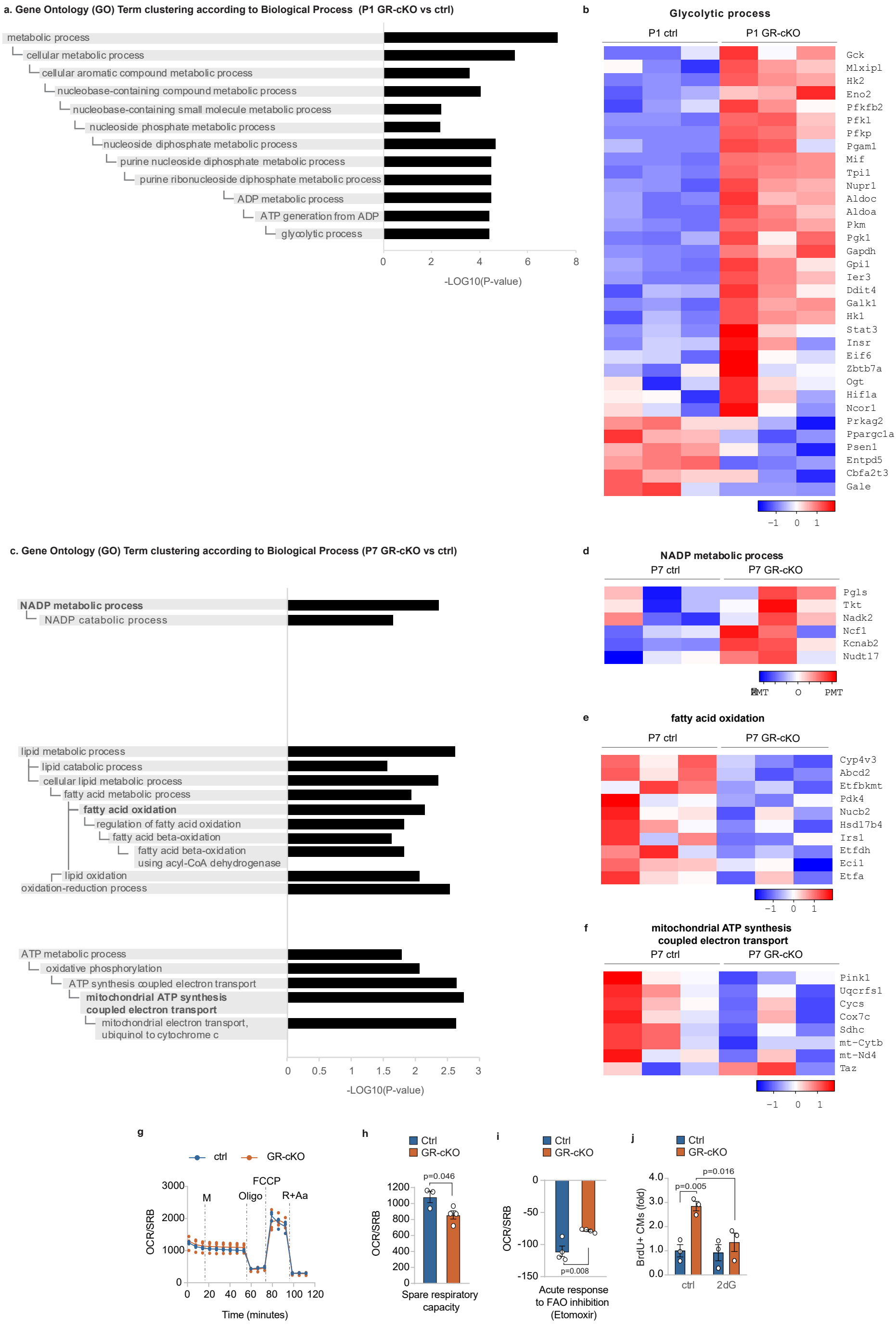
a. Gene Ontology (GO) Term clustering according to Biological Process (P1 GR-cKO vs ctrl)
metabolic process
cellular metabolic process
cellular aromatic compound metabolic process
nucleobase-containing compound metabolic process
nucleobase-containing small molecule metabolic process
nucleoside phosphate metabolic process
nucleoside diphosphate metabolic process
purine nucleoside diphosphate metabolic process
purine ribonucleoside diphosphate metabolic process
ADP metabolic process
ATP generation from ADP
glycolytic process
0 2 4 6 8
-LOG10(P-value)
b
Glycolytic process
P1 ctrl
P1 GR-cKO
Gck
Mlxipl
Hk2
Eno2
Pfkfb2
Pfkl
Pfkp
Pgam1
Mif
Tpi1
Nupr1
Aldoc
Aldoa
Pkm
Pgk1
Gapdh
Gpi1
Ier3
Ddit4
Galk1
Hk1
Stat3
Insr
Eif6
Zbtb7a
Ogt
Hif1a
Ncor1
Prkag2
Ppargc1a
Psen1
Entpd5
Cbfa2t3
Gale
−1 0 1
c. Gene Ontology (GO) Term clustering according to Biological Process (P7 GR-cKO vs ctrl)
NADP metabolic process
NADP catabolic process
lipid metabolic process
lipid catabolic process
cellular lipid metabolic process
fatty acid metabolic process
fatty acid oxidation
regulation of fatty acid oxidation
fatty acid beta-oxidation
fatty acid beta-oxidation using acyl-CoA dehydrogenase
lipid oxidation
oxidation-reduction process
ATP metabolic process
oxidative phosphorylation
ATP synthesis coupled electron transport
mitochondrial ATP synthesis coupled electron transport
mitochondrial electron transport, ubiquinol to cytochrome c
0 0.5 1 1.5 2 2.5 3
-LOG10(P-value)
d
NADP metabolic process
P7 ctrl
P7 GR-cKO
Pgls
Tkt
Nadk2
Ncf1
Kcnab2
Nudt17
PMT 0 PMT
e
fatty acid oxidation
P7 ctrl
P7 GR-cKO
Cyp4v3
Abcd2
Etfbkmt
Pdk4
Nucb2
Hsd17b4
Irs1
Etfdh
Eci1
Etfa
−1 0 1
f
mitochondrial ATP synthesis coupled electron transport
P7 ctrl
P7 GR-cKO
Pink1
Uqcrfs1
Cycs
Cox7c
Sdhc
mt-Cytb
mt-Nd4
Taz
−1 0 1
g
ctrl
GR-cKO
FCCP
M
Oligo
R+Aa
OCR/SRB
Time (minutes)
h
Ctrl
GR-cKO
p=0.046
OCR/SRB
Spare respiratory capacity
i
Ctrl
GR-cKO
OCR/SRB
p=0.008
Acute response to FAO inhibition (Etomoxir)
j
Ctrl
GR-cKO
p=0.016
p=0.005
BrdU+ CMs (fold)
ctrl
2dG

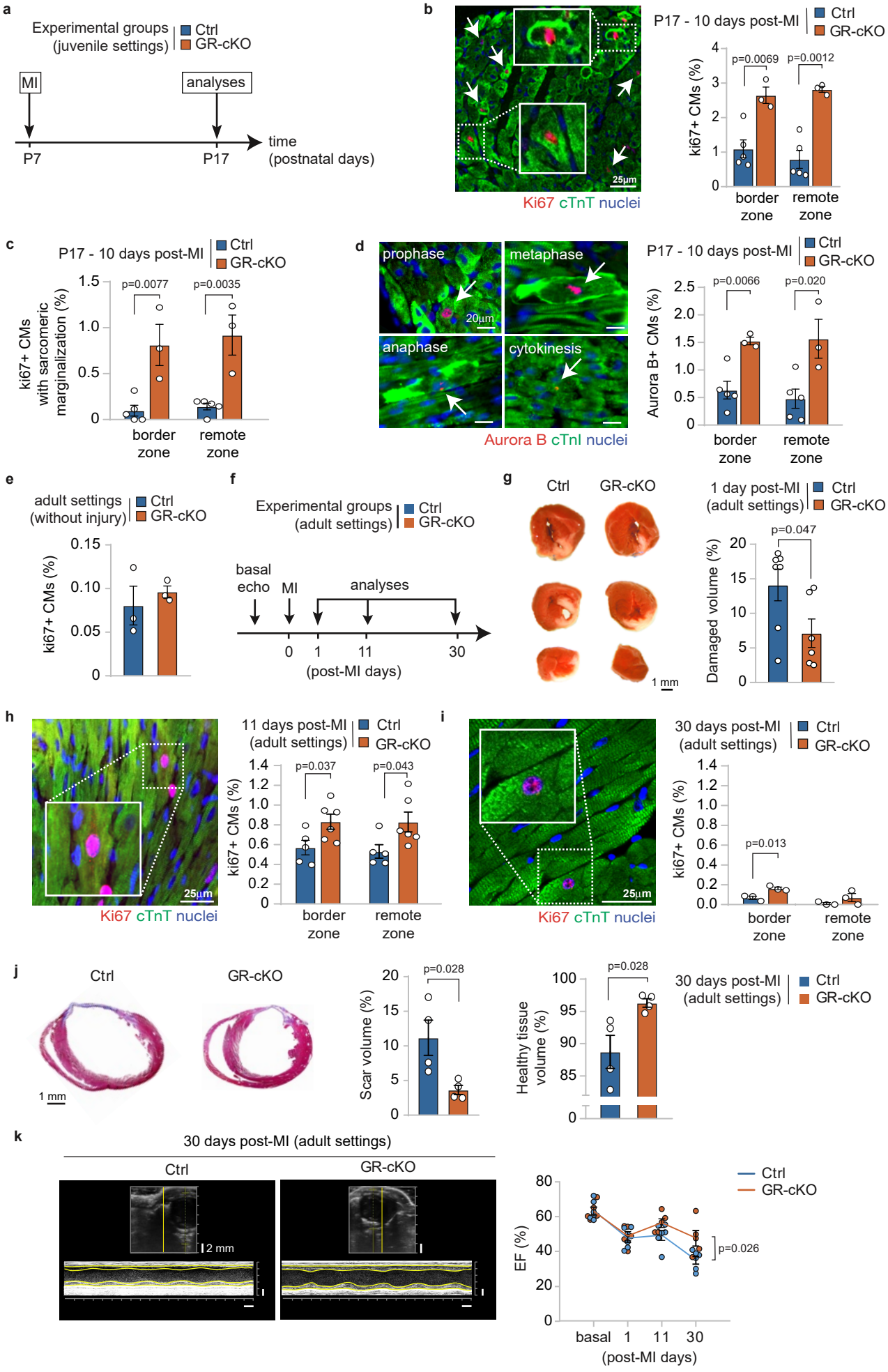
a
Experimental groups (juvenile settings)
Ctrl
GR-cKO
MI
analyses
P7
P17
time (postnatal days)
b
P17 - 10 days post-MI
Ctrl
GR-cKO
ki67+ CMs (%)
p=0.0069
p=0.0012
border zone
remote zone
25µm
Ki67 cTnT nuclei
c
P17 - 10 days post-MI
ki67+ CMs with sarcomeric marginalization (%)
p=0.0077
p=0.0035
border zone
remote zone
d
prophase
metaphase
anaphase
cytokinesis
20µm
Aurora B cTnI nuclei
P17 - 10 days post-MI
Aurora B+ CMs (%)
p=0.0066
p=0.020
border zone
remote zone
e
adult settings (without injury)
Ctrl
GR-cKO
ki67+ CMs (%)
f
Experimental groups (adult settings)
Ctrl
GR-cKO
basal echo
MI
analyses
0
1
11
30
(post-MI days)
g
Ctrl
GR-cKO
1 mm
1 day post-MI (adult settings)
Ctrl
GR-cKO
Damaged volume (%)
p=0.047
h
25µm
Ki67 cTnT nuclei
11 days post-MI (adult settings)
Ctrl
GR-cKO
ki67+ CMs (%)
p=0.037
p=0.043
border zone
remote zone
i
25µm
Ki67 cTnT nuclei
30 days post-MI (adult settings)
Ctrl
GR-cKO
ki67+ CMs (%)
p=0.013
border zone
remote zone
j
Ctrl
GR-cKO
1 mm
Scar volume (%)
p=0.028
Healthy tissue volume (%)
p=0.028
30 days post-MI (adult settings)
Ctrl
GR-cKO
k
30 days post-MI (adult settings)
Ctrl
GR-cKO
2 mm
EF (%)
p=0.026
basal
1
11
30
(post-MI days)

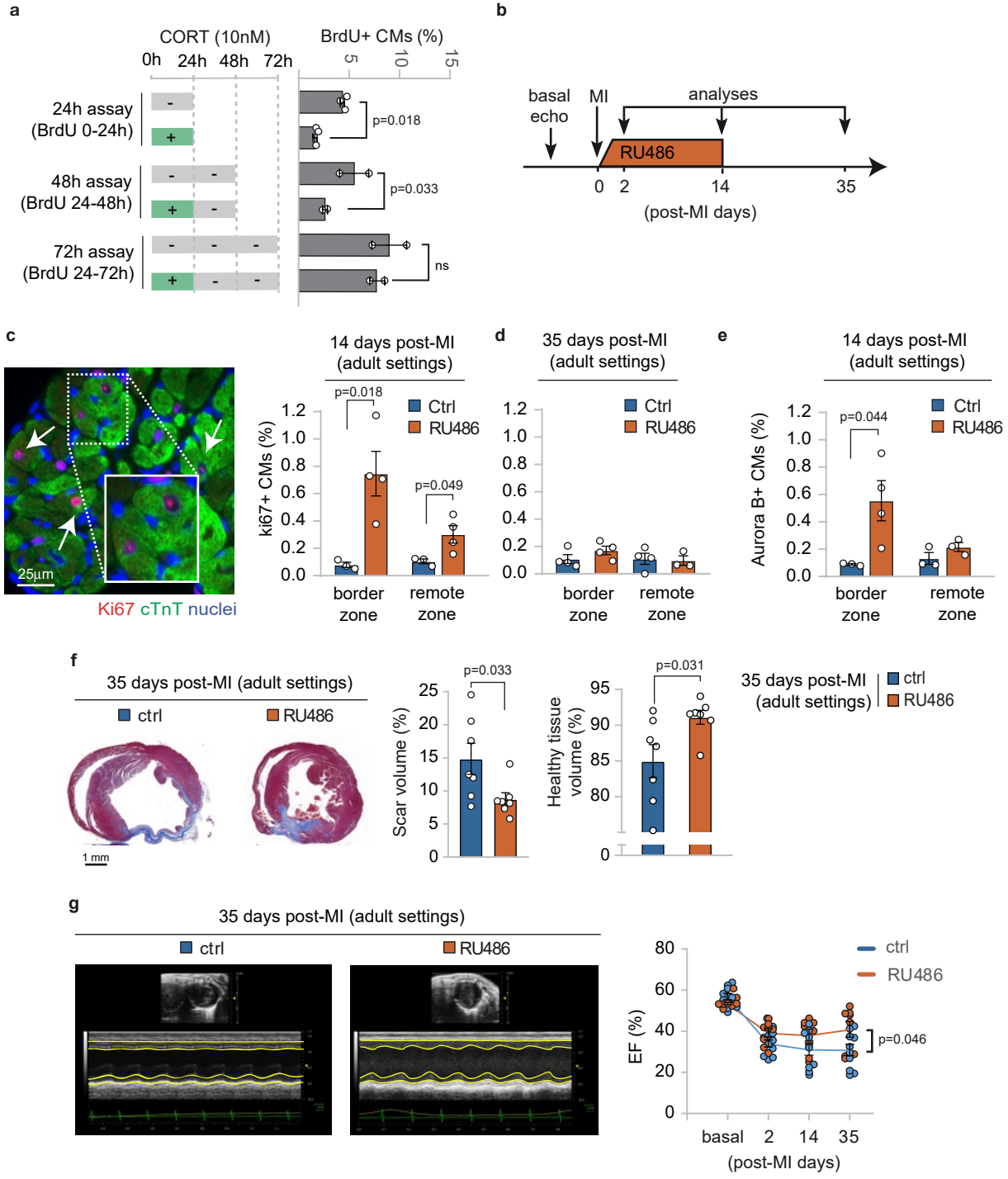
a
CORT (10nM)
0h 24h 48h 72h
BrdU+ CMs (%)
5 10 15
24h assay (BrdU 0-24h)
48h assay (BrdU 24-48h)
72h assay (BrdU 24-72h)
p=0.018
p=0.033
ns
b
basal echo
MI
analyses
RU486
0 2 14 35
(post-MI days)
c
25µm
Ki67 cTnT nuclei
14 days post-MI (adult settings)
ki67+ CMs (%)
Ctrl
RU486
p=0.018
p=0.049
border zone
remote zone
d
35 days post-MI (adult settings)
e
14 days post-MI (adult settings)
Aurora B+ CMs (%)
p=0.044
f
35 days post-MI (adult settings)
ctrl
RU486
1 mm
Scar volume (%)
p=0.033
Healthy tissue volume (%)
p=0.031
g
35 days post-MI (adult settings)
EF (%)
p=0.046
basal 2 14 35
(post-MI days)

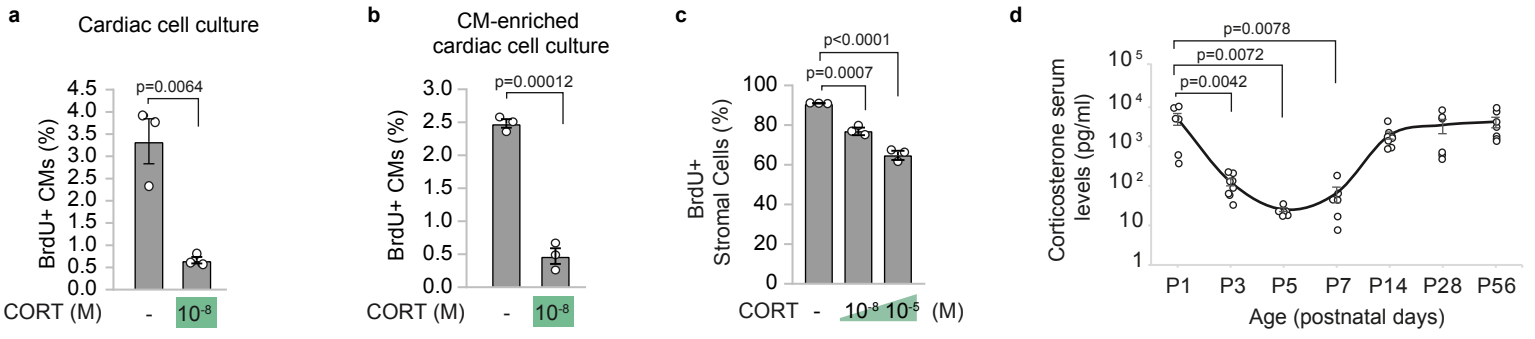
a
Cardiac cell culture
p=0.0064
BrdU+ CMs (%)
4.5
4.0
3.5
3.0
2.5
2.0
1.5
1.0
0.5
0.0
CORT (M)
-
10-8
b
CM-enriched cardiac cell culture
p=0.00012
BrdU+ CMs (%)
3.0
2.5
2.0
1.5
1.0
0.5
0.0
CORT (M)
-
10-8
c
p<0.0001
p=0.0007
BrdU+ Stromal Cells (%)
100
80
60
40
20
0
CORT
-
10-8
10-5
(M)
d
p=0.0078
p=0.0072
p=0.0042
Corticosterone serum levels (pg/ml)
10 5
10 4
10 3
10 2
10
1
P1
P3
P5
P7
P14
P28
P56
Age (postnatal days)

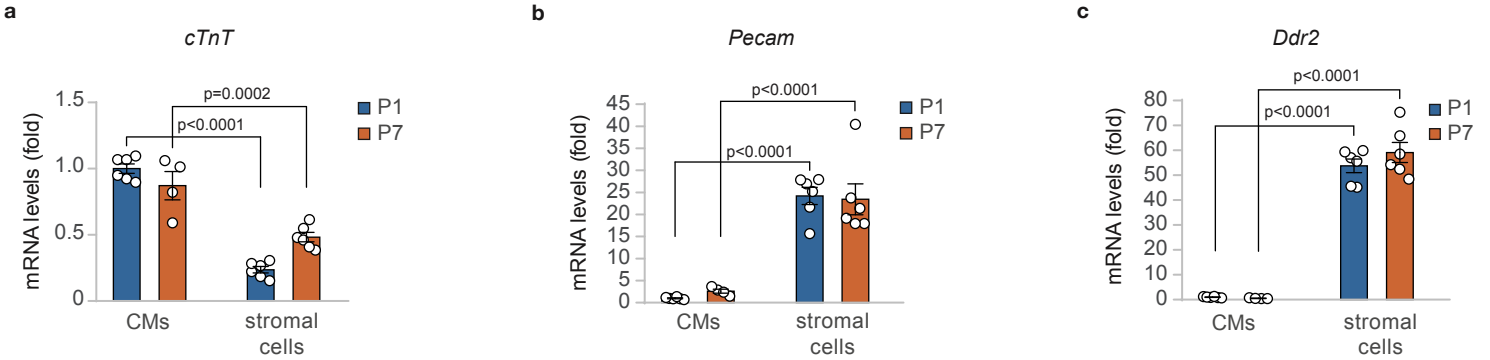
a
cTnT
mRNA levels (fold)
1.5
1.0
0.5
0
p=0.0002
p<0.0001
P1
P7
CMs
stromal cells
b
Pecam
mRNA levels (fold)
45
40
35
30
25
20
15
10
5
0
p<0.0001
p<0.0001
P1
P7
CMs
stromal cells
c
Ddr2
mRNA levels (fold)
80
70
60
50
40
30
20
10
0
p<0.0001
p<0.0001
P1
P7
CMs
stromal cells

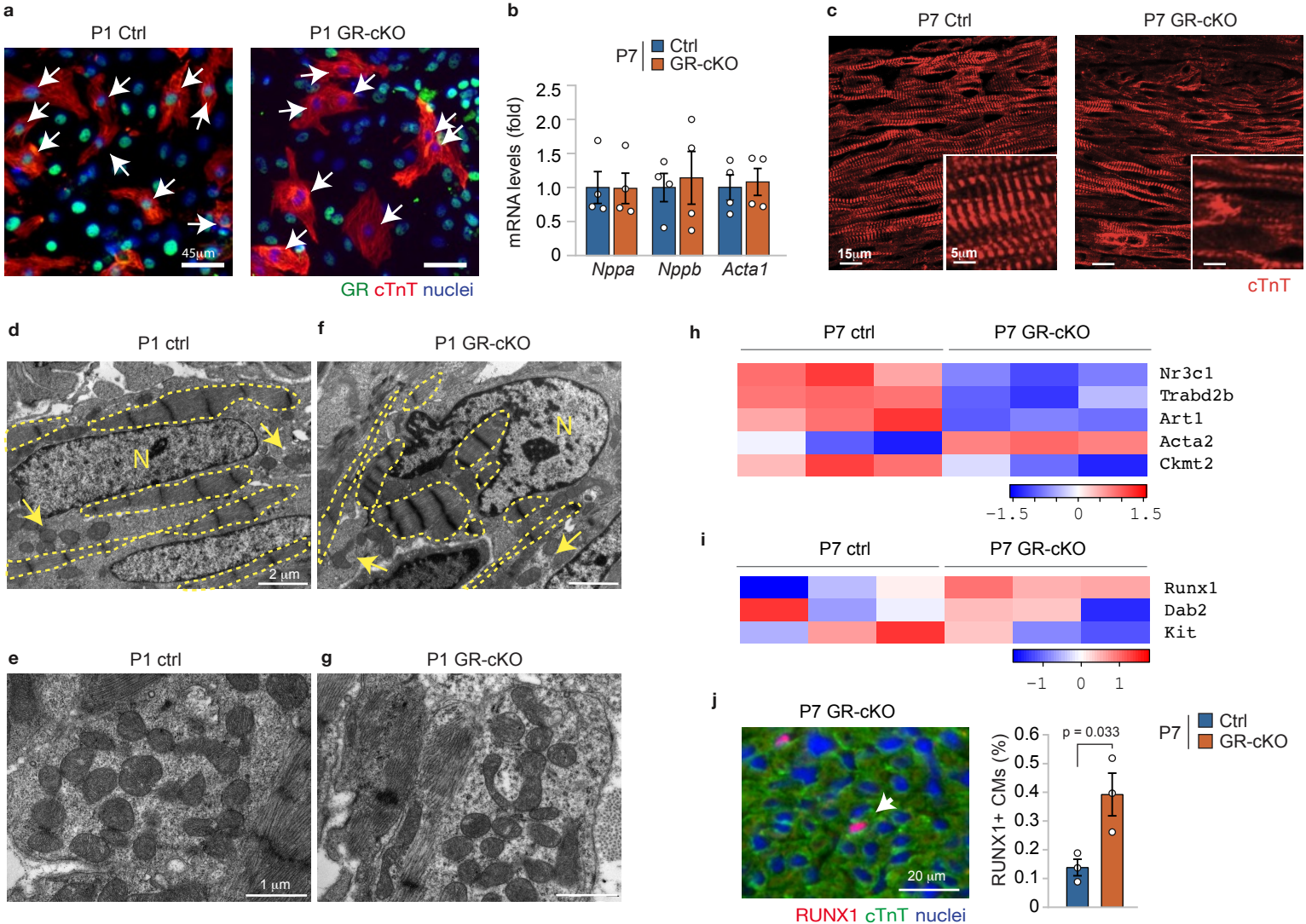
a
P1 Ctrl
P1 GR-cKO
45µm
GR cTnT nuclei
b
P7
Ctrl
GR-cKO
mRNA levels (fold)
2.5
2.0
1.5
1.0
0.5
0
Nppa
Nppb
Acta1
c
P7 Ctrl
P7 GR-cKO
15µm
5µm
cTnT
d
P1 ctrl
N
2 µm
f
P1 GR-cKO
N
e
P1 ctrl
1 µm
g
P1 GR-cKO
h
P7 ctrl
P7 GR-cKO
Nr3c1
Trabd2b
Art1
Acta2
Ckmt2
-1.5
0
1.5
i
P7 ctrl
P7 GR-cKO
Runx1
Dab2
Kit
-1
0
1
j
P7 GR-cKO
20 µm
RUNX1 cTnT nuclei
RUNX1+ CMs (%)
0.6
0.5
0.4
0.3
0.2
0.1
0
p = 0.033
P7
Ctrl
GR-cKO

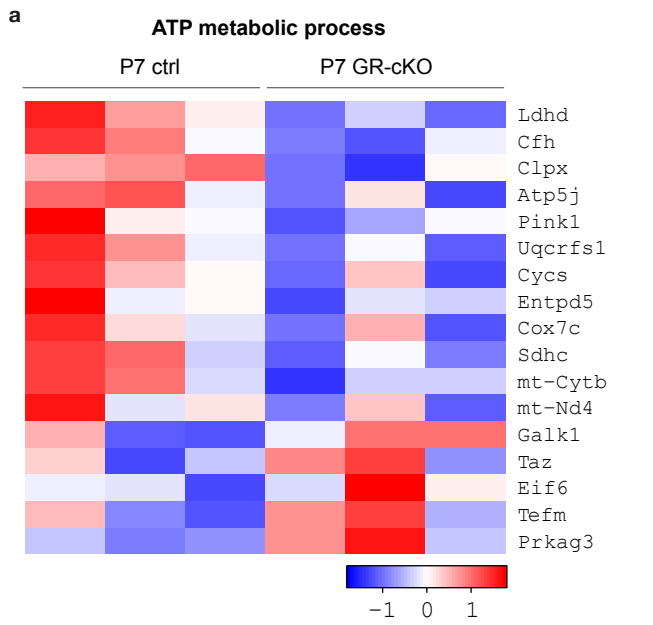
a
ATP metabolic process
P7 ctrl
P7 GR-cKO
Ldhd
Cfh
Clpx
Atp5j
Pink1
Uqcrfs1
Cycs
Entpd5
Cox7c
Sdhc
mt-Cytb
mt-Nd4
Galk1
Taz
Eif6
Tefm
Prkag3
−1 0 1

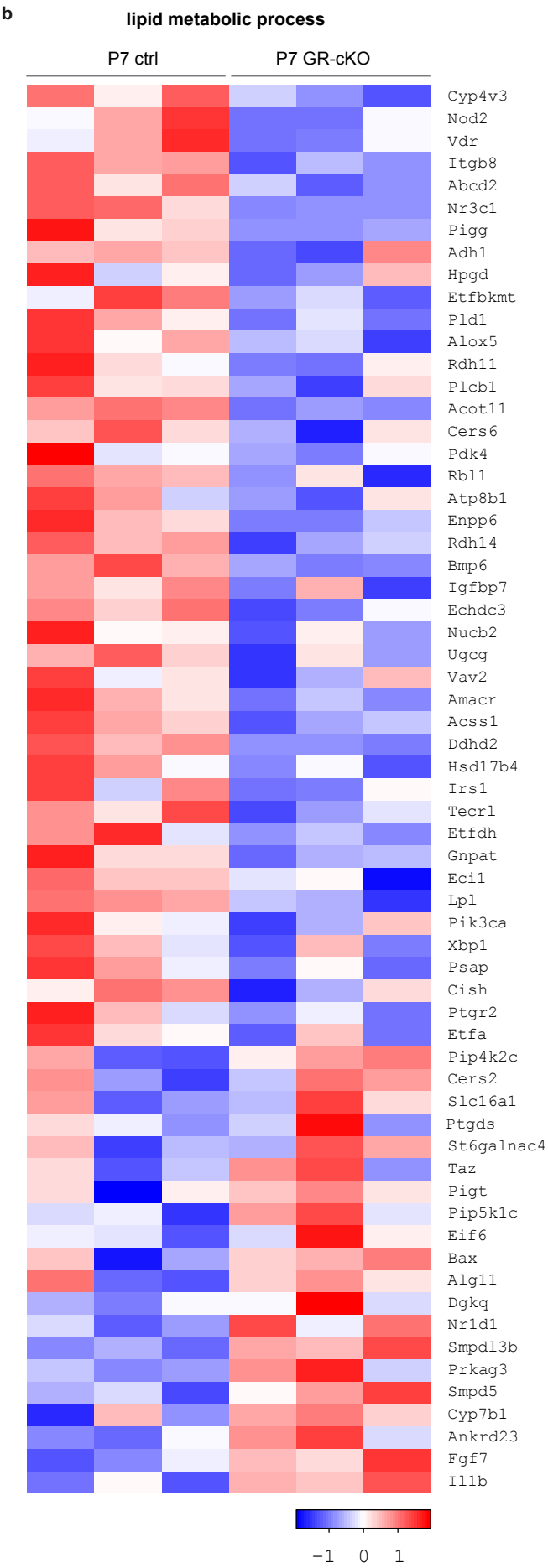
b
lipid metabolic process
P7 ctrl
P7 GR-cKO
Cyp4v3
Nod2
Vdr
Itgb8
Abcd2
Nr3c1
Pigg
Adh1
Hpgd
Etfbkmt
Pld1
Alox5
Rdh11
Plcb1
Acot11
Cers6
Pdk4
Rbl1
Atp8b1
Enpp6
Rdh14
Bmp6
Igfbp7
Echdc3
Nucb2
Ugcg
Vav2
Amacr
Acss1
Ddhd2
Hsd17b4
Irs1
Tecrl
Etfdh
Gnpat
Eci1
Lpl
Pik3ca
Xbp1
Psap
Cish
Ptgr2
Etfa
Pip4k2c
Cers2
Slc16a1
Ptgds
St6galnac4
Taz
Pigt
Pip5k1c
Eif6
Bax
Alg11
Dgkq
Nr1d1
Smpdl3b
Prkag3
Smpd5
Cyp7b1
Ankrd23
Fgf7
Il1b
−1 0 1

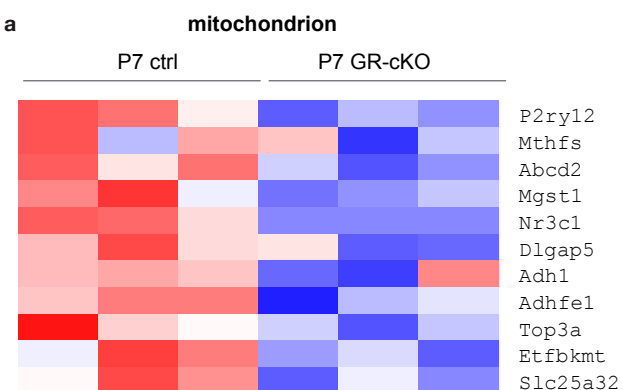
a
mitochondrion
P7 ctrl
P7 GR-cKO
P2ry12
Mthfs
Abcd2
Mgst1
Nr3c1
Dlgap5
Adh1
Adhfe1
Top3a
Etfbkmt
Slc25a32
Ldhd
Hlcs
Acot11
Pin4
Aldh7a1
Pdk4
Ppm1e
Nubpl
Uros
Rdh14
Acyp2
Pdp2
Oxld1
Ide
Echdc3
Ckmt2
Amacr
Cebpzos
Timm21
Acss1
Shmt1
Gng5
Hsd17b4
Dbt
Clpx
Pxmp2
Atp5j
Etfdh
Gnpat
Eci1
Pmpcb
Dcaf5
Ank2
Nbr1
Rpl35a
Psap
Pink1
Ammecr1
Tango2
Uqcrfs1
Aldh1b1
Ptgr2
Sord
Cycs
Ndufa1
Etfa
Cox7c
Cox7b
Sdhc
mt-Cytb
Slc25a4
mt-Nd4
−1 0 1

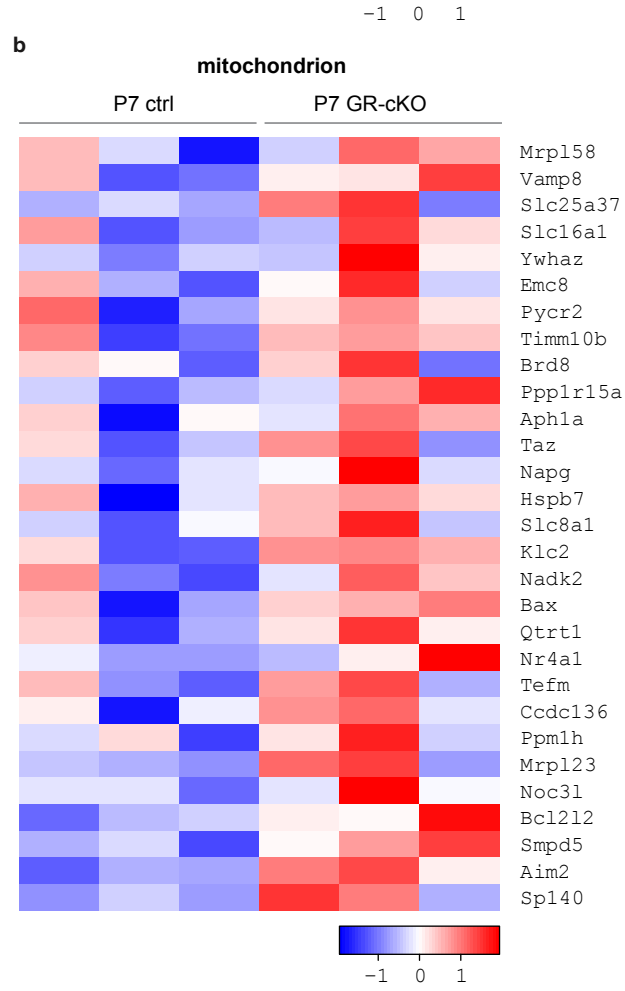
b
mitochondrion
P7 ctrl
P7 GR-cKO
Mrpl58
Vamp8
Slc25a37
Slc16a1
Ywhaz
Emc8
Pycr2
Timm10b
Brd8
Ppp1r15a
Aph1a
Taz
Napg
Hspb7
Slc8a1
Klc2
Nadk2
Bax
Qtrt1
Nr4a1
Tefm
Ccdc136
Ppm1h
Mrpl23
Noc3l
Bcl2l2
Smpd5
Aim2
Sp140
−1 0 1

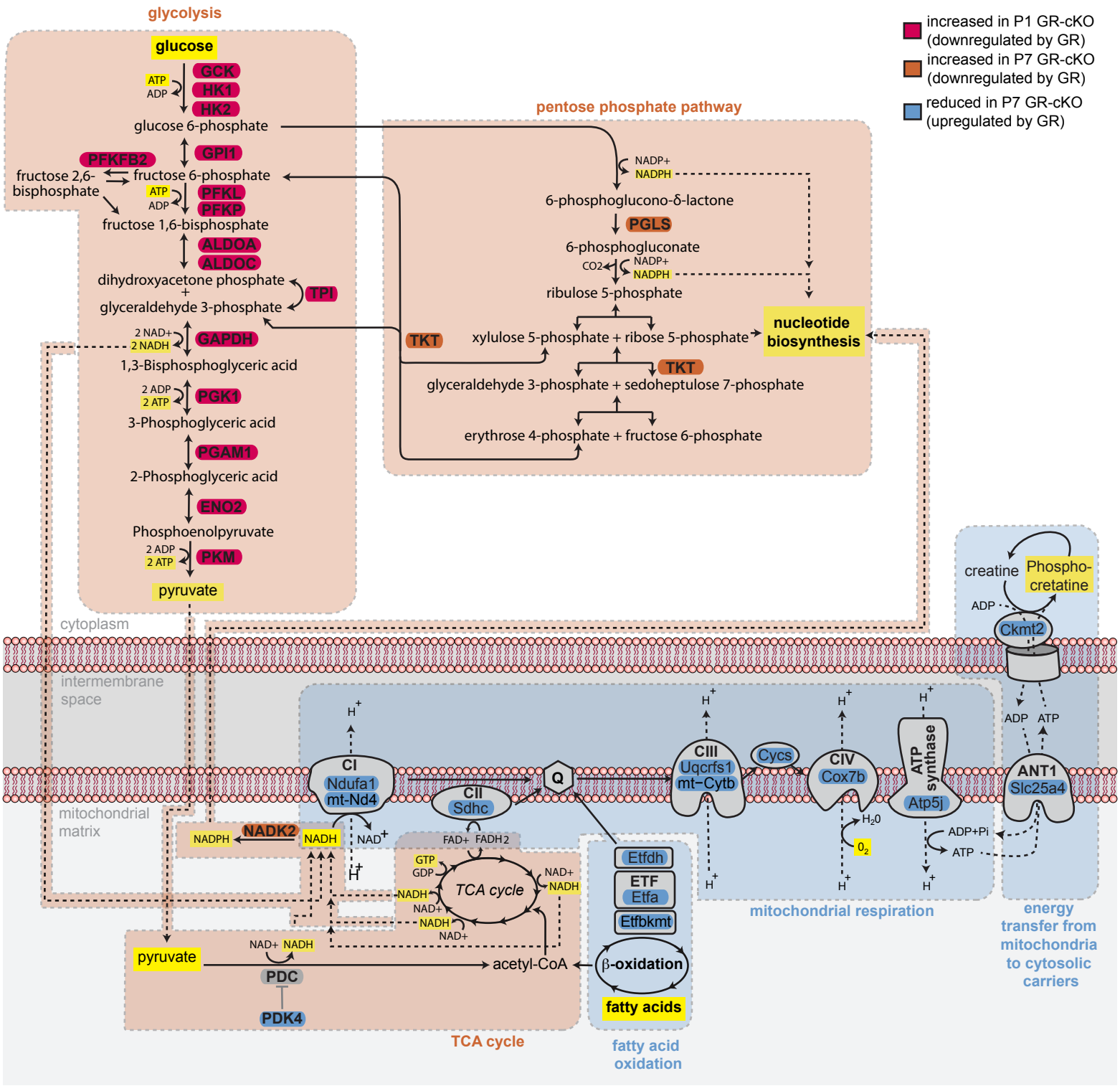
glycolysis
glucose
ATP
ADP
GCK
HK1
HK2
glucose 6-phosphate
GPI1
PFKFB2
fructose 2,6-bisphosphate
fructose 6-phosphate
ATP
ADP
PFKL
PFKP
fructose 1,6-bisphosphate
ALDOA
ALDOC
dihydroxyacetone phosphate
+
glyceraldehyde 3-phosphate
TPI
2 NAD+
2 NADH
GAPDH
1,3-Bisphosphoglyceric acid
2 ADP
2 ATP
PGK1
3-Phosphoglyceric acid
PGAM1
2-Phosphoglyceric acid
ENO2
Phosphoenolpyruvate
2 ADP
2 ATP
PKM
pyruvate
pentose phosphate pathway
NADP+
NADPH
6-phosphoglucono-δ-lactone
PGLS
6-phosphogluconate
CO2
NADP+
NADPH
ribulose 5-phosphate
TKT
xylulose 5-phosphate + ribose 5-phosphate
nucleotide biosynthesis
TKT
glyceraldehyde 3-phosphate + sedoheptulose 7-phosphate
erythrose 4-phosphate + fructose 6-phosphate
increased in P1 GR-cKO (downregulated by GR)
increased in P7 GR-cKO (downregulated by GR)
reduced in P7 GR-cKO (upregulated by GR)
creatine
Phospho-cretatine
ADP
Ckmt2
cytoplasm
intermembrane space
mitochondrial matrix
H+
CI
Ndufa1
mt-Nd4
CII
Sdhc
Q
CIII
Uqcrfs1
mt-Cytb
Cycs
CIV
Cox7b
ATP synthase
Atp5j
ANT1
Slc25a4
ADP
ATP
NADH
NADK2
NADPH
NAD+
FAD+
FADH2
GTP
GDP
TCA cycle
NAD+
NADH
Etfdh
ETF
Etfa
Etfbkmt
β-oxidation
fatty acids
H2O
O2
ADP+Pi
ATP
mitochondrial respiration
energy transfer from mitochondria to cytosolic carriers
pyruvate
NAD+
NADH
PDC
PDK4
acetyl-CoA
TCA cycle
fatty acid oxidation

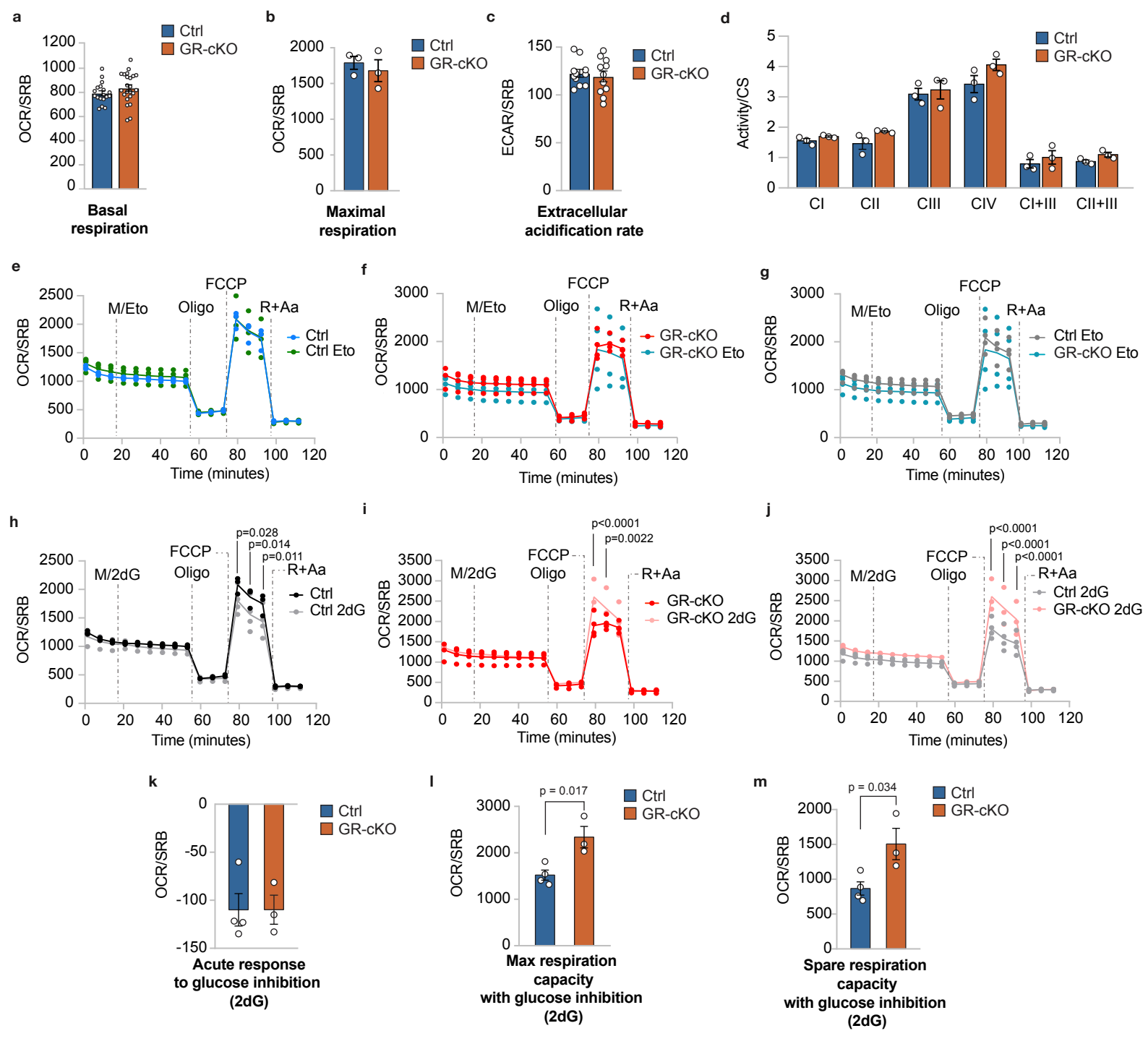
a
OCR/SRB
Ctrl
GR-cKO
Basal respiration
b
OCR/SRB
Ctrl
GR-cKO
Maximal respiration
c
ECAR/SRB
Ctrl
GR-cKO
Extracellular acidification rate
d
Activity/CS
Ctrl
GR-cKO
CI
CII
CIII
CIV
CI+III
CII+III
e
OCR/SRB
M/Eto
Oligo
FCCP
R+Aa
Ctrl
Ctrl Eto
Time (minutes)
f
OCR/SRB
M/Eto
Oligo
FCCP
R+Aa
GR-cKO
GR-cKO Eto
Time (minutes)
g
OCR/SRB
M/Eto
Oligo
FCCP
R+Aa
Ctrl Eto
GR-cKO Eto
Time (minutes)
h
OCR/SRB
M/2dG
Oligo
FCCP
R+Aa
p=0.028
p=0.014
p=0.011
Ctrl
Ctrl 2dG
Time (minutes)
i
OCR/SRB
M/2dG
Oligo
FCCP
R+Aa
p<0.0001
p=0.0022
GR-cKO
GR-cKO 2dG
Time (minutes)
j
OCR/SRB
M/2dG
Oligo
FCCP
R+Aa
p<0.0001
p<0.0001
p<0.0001
Ctrl 2dG
GR-cKO 2dG
Time (minutes)
k
OCR/SRB
Ctrl
GR-cKO
Acute response to glucose inhibition (2dG)
l
OCR/SRB
p = 0.017
Ctrl
GR-cKO
Max respiration capacity with glucose inhibition (2dG)
m
OCR/SRB
p = 0.034
Ctrl
GR-cKO
Spare respiration capacity with glucose inhibition (2dG)

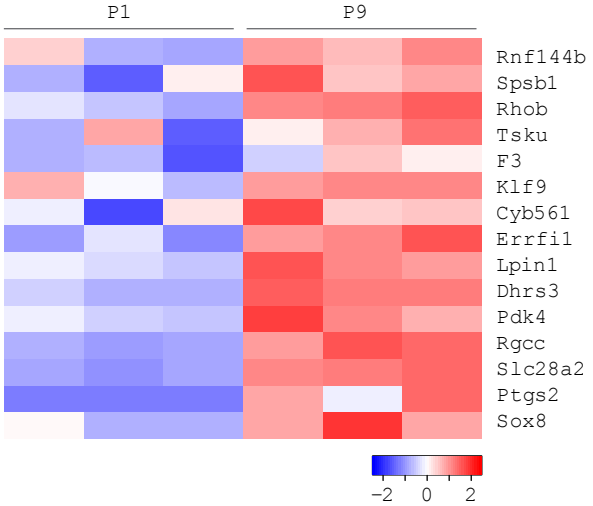
P1
P9
Rnf144b
Spsb1
Rhob
Tsku
F3
Klf9
Cyb561
Errfi1
Lpin1
Dhrs3
Pdk4
Rgcc
Slc28a2
Ptgs2
Sox8
−2
0
2

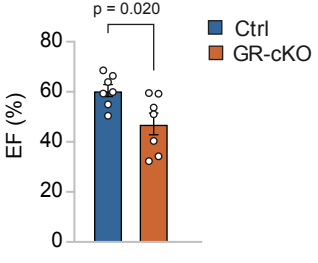
p = 0.020
Ctrl
GR-cKO
EF (%)
80
60
40
20
0

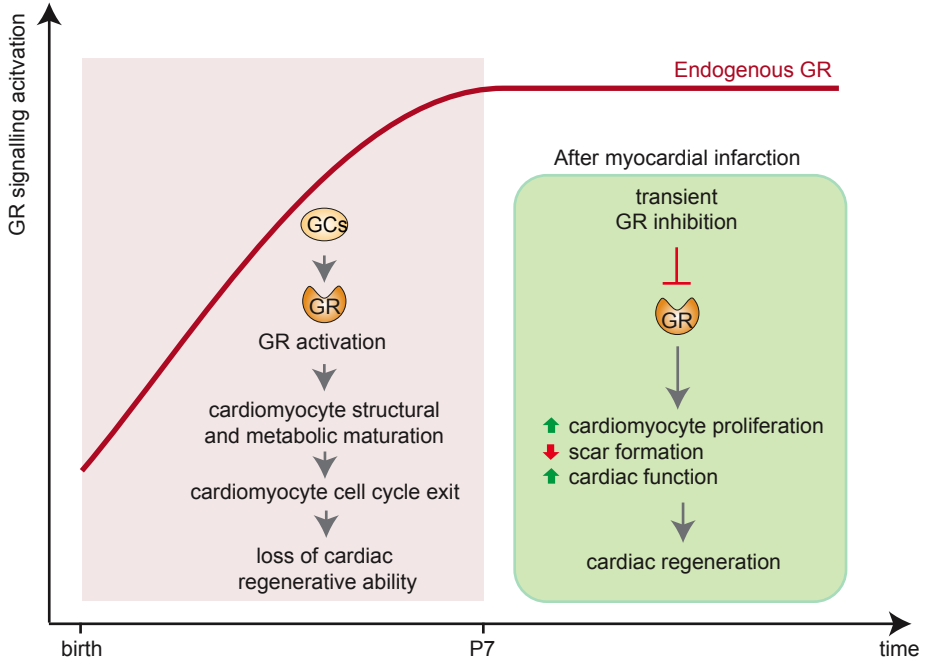
GR signalling acitvation
Endogenous GR
GCs
GR
GR activation
cardiomyocyte structural
and metabolic maturation
cardiomyocyte cell cycle exit
loss of cardiac
regenerative ability
After myocardial infarction
transient
GR inhibition
GR
cardiomyocyte proliferation
scar formation
cardiac function
cardiac regeneration
birth
P7
time

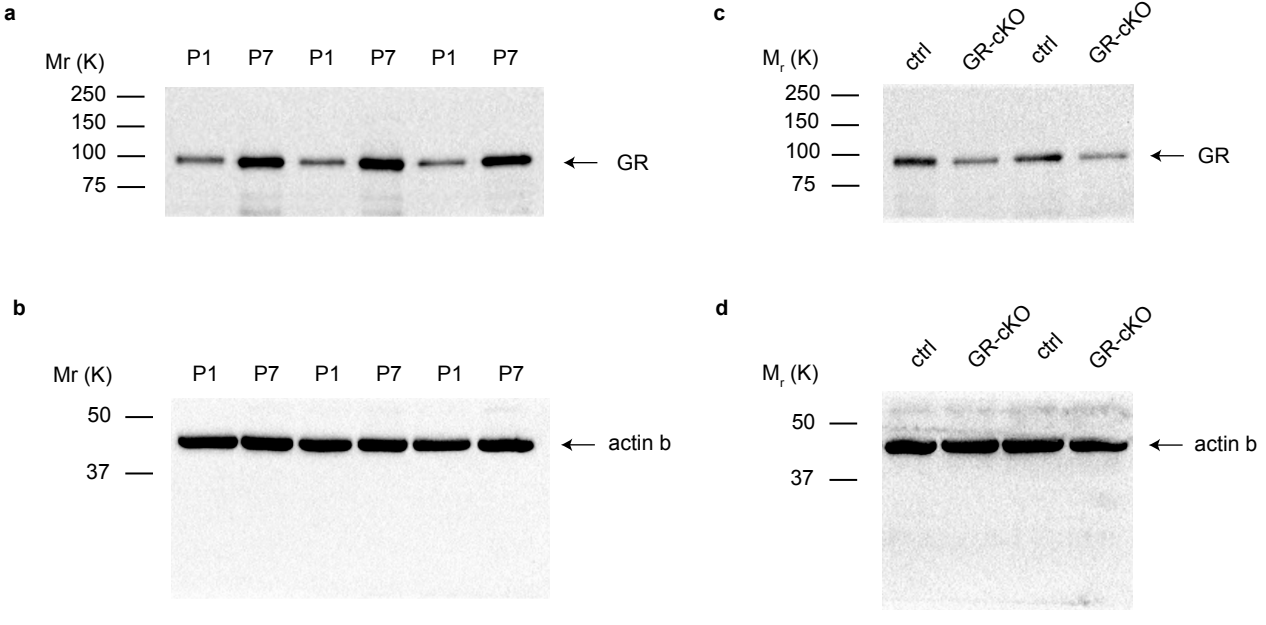
a
Mr (K)
P1
P7
P1
P7
P1
P7
250
150
100
75
GR
b
Mr (K)
P1
P7
P1
P7
P1
P7
50
37
actin b
c
Mr (K)
ctrl
GR-cKO
ctrl
GR-cKO
250
150
100
75
GR
d
Mr (K)
ctrl
GR-cKO
ctrl
GR-cKO
50
37
actin b